MASTER COPY KEEP THIS COPY FOR REPRODUCTION PURPOSES

REPORT DOCUMENTATION PAGE

Form Approved
OMB No. 0704-0188

1. AGENCY USE ONLY (Leave blank)	2. REPORT DATE	3. REPORT TYPE AND DATES COVERED
	November 23, 1994	Final Report 1 Jan 91 - 30 Sept 94

4. TITLE AND SUBTITLE High- and Low-Frequency Dynamics of Isolated Blades and Rotors with Dynamic Stall and Wake.

5. FUNDING NUMBERS

DAAL03-91-G-0007

6. AUTHOR(S)

Gopal H. Gaonkar

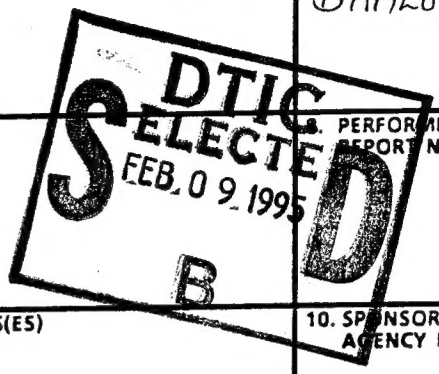

7. PERFORMING ORGANIZATION NAME(S) AND ADDRESS(ES)

Department of Mechanical Engineering
Florida Atlantic University
Boca Raton, FL 33431

8. PERFORMING ORGANIZATION REPORT NUMBER

9. SPONSORING/MONITORING AGENCY NAME(S) AND ADDRESS(ES)

U. S. Army Research Office
P. O. Box 12211
Research Triangle Park, NC 27709-2211

10. SPONSORING/MONITORING AGENCY REPORT NUMBER

ARO 28123.10-EG

11. SUPPLEMENTARY NOTES

The view, opinions and/or findings contained in this report are those of the author(s) and should not be construed as an official Department of the Army position, policy, or decision, unless so designated by other documentation.

12a. DISTRIBUTION/AVAILABILITY STATEMENT

Approved for public release; distribution unlimited.

12b. DISTRIBUTION CODE

13. ABSTRACT *(Maximum 200 words)* This report investigates the effects of dynamic stall and three-dimensional wake on the trim results of control inputs and periodic responses and on the damping levels of isolated hingeless rotors. The investigation covers three items: 1) the convergence characteristics of trim and damping with respect to the number of harmonics of the wake model in the presence of dynamic stall; 2) a parametric study of trim and damping over a broad range of system parameters such as thrust level and advance ratio, and 3) a comprehensive correlation with the measured lag-regressive-mode damping. The correlation includes near-zero thrust conditions in hover and forward flight to high-thrust and highly stalled conditions in forward flight with advance ratio as high as 0.55 and shaft angle as high as 20^0. The convergence characteristics and the parametric study are based on a three-bladed isolated rotor in propulsive trim; the cantilever blades have flap bending, lag bending and torsion degrees of freedom. In the correlation study, the root-flexure-blade assembly of the experimental rotor is modeled by an offset-hinged, rigid flap-lag model and by three elastic blade models, which differ in modeling the root flexure. The experimental rotor is soft inplane and operated untrimmed. The ONERA dynamic stall models of lift, drag and pitching moment and a finite-state three-dimensional wake model are used. The control inputs and periodic responses as well as the Floquet transition matrix about that response are obtained by periodic shooting with damped Newton iteration. The damping levels are generated from a full Floquet analysis that includes all the structural and aerodynamic states in trim analysis and eigenanalysis. For lag damping predictions in the presence of dynamic stall, at least nine wake harmonics are required even for the low-frequency lag-regressive mode. Moreover, dynamic stall and wake effects are appreciable on control inputs, periodic responses and damping levels, and including these effects appreciably improves the correlation.

14. SUBJECT TERMS	15. NUMBER OF PAGES
Dynamic Stall, Dynamic Wake, Trim, Stability, Lag Damping, Correlation, Hingeless Rotor	49
	16. PRICE CODE

17. SECURITY CLASSIFICATION OF REPORT	18. SECURITY CLASSIFICATION OF THIS PAGE	19. SECURITY CLASSIFICATION OF ABSTRACT	20. LIMITATION OF ABSTRACT
UNCLASSIFIED	UNCLASSIFIED	UNCLASSIFIED	UL

Contents

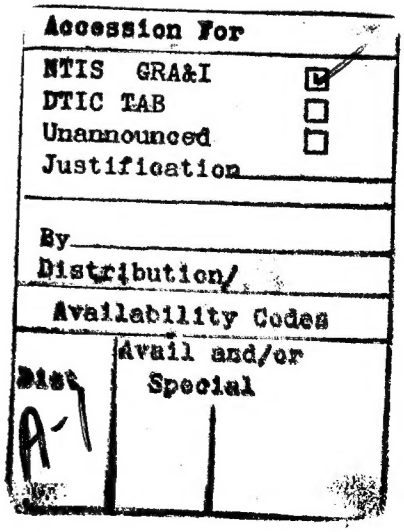

Summary

This report investigates the effects of dynamic stall and three-dimensional wake on the trim results of control inputs and periodic responses and on the damping levels of isolated hingeless rotors. The investigation covers three items: 1) the convergence characteristics of trim and damping with respect to the number of harmonics of the wake model in the presence of dynamic stall; 2) a parametric study of trim and damping over a broad range of system parameters such as thrust level and advance ratio, and 3) a comprehensive correlation with the measured lag-regressive-mode damping. The correlation includes near-zero thrust conditions in hover and forward flight to high-thrust and highly stalled conditions in forward flight with advance ratio as high as 0.55 and shaft angle as high as 20^0. The convergence characteristics and the parametric study are based on a three-bladed isolated rotor in propulsive trim; the cantilever blades have flap bending, lag bending and torsion degrees of freedom. In the correlation study, the root-flexure-blade assembly of the experimental rotor is modeled by an offset-hinged, rigid flap-lag model and by three elastic blade models, which differ in modeling the root flexure. The experimental rotor is soft inplane and operated untrimmed. The ONERA dynamic stall models of lift, drag and pitching moment and a finite-state three-dimensional wake model are used. The control inputs and periodic responses as well as the Floquet transition matrix about that response are obtained by periodic shooting with damped Newton iteration. The damping levels are generated from a full Floquet analysis that includes all the structural and aerodynamic states in trim analysis and eigenanalysis. For lag damping predictions in the presence of dynamic stall, at least nine wake harmonics are required even for the low-frequency lag-regressive mode. Moreover, dynamic stall and wake effects are appreciable on control inputs, periodic responses and damping levels, and including these effects appreciably improves the correlation.

Notation

Unless otherwise stated, the symbols below are dimensionless:

a	linear lift curve slope, (rad^{-1})
a_d, a_m	damping factors in dynamic stall drag and pitching moment models
b	airfoil semi-chord, $(1/R)$
c, c	airfoil chord, (m); airfoil chord, $(1/R)$
C_d, C_{d_0}	airfoil sectional drag coefficient and constant profile drag coefficient
C_l, C_m	airfoil lift and pitching moment coefficients
C_{m_0}	airfoil pitching moment coefficient at zero angle of attack
C_T	thrust coefficient
C_T/σ_s	thrust level
e	phase shift parameter in dynamic stall lift model
E_d, E_m	phase shift parameters in dynamic stall drag and pitching moment models
$\overline{f}$	equivalent flat plate area of parasite drag
j	polynomial number
k	b/x
L_i	blade sectional lift of the i-th blade, (N/m)
L_x, L_y	local aerodynamic forces (Fig. 1), $(1/\rho b\Omega^2 R^3)$
L_0	apparent mass lift normal to the chord line, $(1/\rho b\Omega^2 R^3)$
$\mathbf{L}_c, \mathbf{L}_s$	influence coefficient matrices
m	harmonic number
M	aerodynamic pitching moment, $(1/\rho b\Omega^2 R^4 \mathrm{c})$; also number of harmonics in the wake model
M_0	noncirculatory aerodynamic pitching moment per unit length, $(1/\rho b\Omega^2 R^4 \mathrm{c})$
$\mathbf{M}$	mass matrix
n	polynomial number
$\overline{P}_n^m(\overline{r}_i)$	normalized Lengendre polynomial (n, m) of the first kind
Q	number of blades
r	harmonic number

r_d, r_m	frequency parameters in dynamic stall drag and pitching moment models
$\bar{r}_i$	radial station of the i-th blade, $(1/R)$
R	rotor radius, (m)
S	number of radial shape functions
t	time parameter
U	resultant air velocity at a blade station (Fig. 1), $(1/\Omega R)$
V	inflow parameter
V_t	total inflow parameter
V_1, V_2	first and second lag mode generalized coordinates
$\mathbf{V}$	diag $\{V_t, V, V, \ldots, V\}$
w, d	dynamic stall lift frequency and damping parameters
W_1, W_2	first and second flap mode generalized coordinates
x	radial distance measured from the rotor center, $(1/R)$
α	blade airfoil section angle of attack, (rad)
α_j^r, β_j^r	wake states
α_s	shaft tilt angle, (deg, rad)
γ	Lock number (blade inertia parameter)
Γ	circulation per unit length, UC_l
Γ_d	circulation-like drag per unit length, UC_d
Γ_m	circulation-like pitching moment per unit length, UC_m
δ	pitch-rate coefficient, (rad^{-1})
δ_m	pitching-moment parameter
$\dot{\varepsilon}$	airfoil rotation rate with respect to airmass
θ_0	collective pitch angle, (deg, rad)
θ_c	longitudinal cyclic pitch angle, (rad)
θ_s	lateral cyclic pitch angle, (rad)
λ	time-delay parameter
$\lambda(\bar{r}_i, \psi_i, t)$	downwash on the i-th blade
λ_m	thrust induced inflow
λ_t	total inflow

μ	advance ratio
ϕ_1, ϕ_2	first and second torsion mode generalized coordinates
$\phi_j^r(\overline{r}_i)$	radial shape functions
	$\phi_j^r(\overline{r}_i) = \frac{1}{\nu} P_j^r(\nu)\,; \nu = \sqrt{(1-\overline{r}_i^2)}$
σ	damping level or real part of characteristic exponent, $(1/sec)$
σ_s	rotor solidity
ψ_i	azimuthal location of the i-th blade
ρ	air density (kg/m^3)
ω_β	flap natural frequency, rotating
ω_ζ	lag natural frequency, rotating
ω_ϕ	torsion natural frequency, rotating
Ω	rotor angular speed, (rad/sec)
τ_n^{mc}, τ_n^{ms}	inflow forcing functions
$(\,)_1, (\,)_2$	unstalled and stalled components
$(\,)_x, (\,)_y$	x and y components
$\dot{(\,)}$	time derivative of $(\,)$
$\approx$	approximately equal to

List of Figures

1 Introduction

The current capability to predict helicopter lag damping needs significant improvements. Four considerations make the prediction difficult and motivate the present investigation based on Floquet theory. First, drag, induced drag and Coriolis forces are delicately balanced in the inplane direction. Therefore, from hovering to high-speed flights, a wake representation that goes well beyond dynamic-inflow and lift-deficiency-type approximations is required (Ref. 1). Second, with increasing demand on the stability margins of high-speed and highly maneuverable helicopters, high-thrust conditions in forward flight become increasingly important. Thus, the complex phenomenon of dynamic stall becomes an issue (Refs. 2-4) and needs to be accounted for as well. Third, lag-damping prediction is sensitive to modeling the rotor system and its flow field. It is also sensitive to the accuracy of computing the control inputs and the corresponding periodic forced responses from trim analysis, the Floquet transition matrix about that trim solution and the eigenvalues of this matrix. Thus, it is important that a consistent sophistication is maintained from modeling to trim analysis to eigenanalysis. Often this requires that all the structural and aerodynamic states are included not only in trim analysis but also in eigenanalysis (Ref. 5). This is a demanding and expensive exercise; with lag-bending, flap-bending and torsional degrees of freedom, even simplified research models of multiblade rotors with wake and stall dynamics routinely lead to nearly 300 structural and aerodynamic states for converged results. Fourth, given the complexity of the rotor system and its flow field, it becomes necessary that the predictions are checked out against a broad range of model test data. Currently such test data are severely limited. Although not typical of operational rotors, the database due to McNulty is an exception (Ref. 6). It has nearly 2000 data points and is comprehensive to include near-zero thrust conditions in hover and forward flight as well as high-thrust and highly stalled conditions in forward flight ($0 \leq \mu \leq 0.55, 0^0 \leq \theta_0 \leq 6^0, 0^0 \leq \alpha_s \leq 20^0$); for details see Refs. 2 and 7.

Given this background, we review the aeroelastic stability studies with dynamic stall and/or three-dimensional wake modeling. The use of both stall and three-dimensional wake modeling is almost routine in loads and vibration studies. By comparison their use is far less common in stability studies. Perhaps the first study to consider their use is due to

Torok and Chopra (Ref. 4), who also provide a review of aeroelastic stability modeling through 1991. However, in Ref. 4, stall and free wake are included in trim analysis, but they are frozen in dynamic perturbation. Thus, the important effects of wake and stall on trim analysis are included, but their effects on eigenanalysis are not. Moreover, Ref. 4 uses only a lightly loaded section of the database of Ref. 6 (shaft tilt $\alpha_s \leq 10^0$ and collective pitch $\theta_0 \leq 3^0$). Thus, an appreciable section of the database under high shaft-angle and collective-pitch conditions ($\alpha_s \leq 20^0$ and $\theta_0 \leq 6^0$) is not included. Developments since 1991 include the works of Barwey et al. (Refs. 2 and 3), who use dynamic stall modeling and provide correlation with virtually the complete database of Ref. 6. While a rigid flap-lag model is used in Ref. 2, two elastic flap-lag-torsion models that differ in simulating the root flexure are used in Ref. 3. Manjunath et al. (Ref. 1) use a finite-state three-dimensional wake model and rigid flap-lag modeling. Reference 1 also includes limited correlation with test data of Ref. 6 under low-thrust conditions. The work in Ref. 1 is extended in Ref. 8 to include elastic blade modeling. References 1 and 8 also include a review of aeroelastic stability predictions with the use of dynamic wake modeling.

In this report, we investigate the effects of dynamic stall and wake on the trim prediction of control settings and periodic responses as well as on the damping levels of isolated hingeless rotors. We begin with a convergence study; that is, we investigate, in the presence of dynamic stall, the degree of wake modeling necessary for converged results of trim and damping. We then present a parametric study to demonstrate the effects of dynamic stall and three-dimensional wake on trim and stability. We emphasize that all the structural and aerodynamic states are included in trim analysis and eigenanalysis. This is followed by a comprehensive correlation with the complete database of Ref. 6. To help clarify the aerodynamic aspects of the stability problem, predictions based on the linear, quasisteady stall and dynamic stall theories are included in the parametric and correlation studies. In the correlation, the blade dynamics is described by a rigid blade model as well as by three elastic blade models, which differ in modeling the root-flexure of the experimental rotor (details to follow). The intent here is not so much to compare one structural model with the other; rather it is to help clarify further the aerodynamic aspects without the correlation being masked by the sensitivity of the predictions to structural modeling approximations.

We use the ONERA dynamic stall models of lift, drag and pitching moment (Refs. 9 and 10). The unsteady wake is described by a finite-state three-dimensional wake model (Ref. 11). These stall and wake models are well suited to finite-state representation and perturbations about a trim solution and thereby to Floquet eigenanalysis. This is noteworthy in comparison with a range of other models (*e.g.* free wake model), which, though with proven usage in vibration and performance analyses, do not lend themselves well to eigenanalysis. Thus in summary, the trim and damping predictions are based on a broad range of structural and aerodynamic representations, and the correlation covers a comprehensive database (Ref. 6). Such a work from wake modeling detail to parametric study to correlation should provide a useful reference and demonstrate the strengths and weaknesses of predicting lag mode damping in the presence of dynamic stall.

2 Modeling

A cantilever blade model is used in the convergence and parametric studies of trim and damping. The correlation study requires an adequate model of the root-flexure-blade assembly of the three-blade experimental rotor, which was designed to represent a simple model of a hingeless rotor with spring restrained flap-lag hinges. While the mass and stiffness distributions are essentially uniform for the blade portion, they are highly nonuniform for the root flexure or root beam. According to Ref. 3, the sensitivity of lag-damping predictions to the structural refinements in modeling the root-flexure-blade assembly increases with increasing blade pitch and advance ratio. Therefore, to bracket the extent of this sensitivity to modeling details, we use four models of the root-flexure-blade assembly. They range from a rigid flap-lag blade model to three elastic flap-lag-torsion models, which have identical blade representation but differ in root-flexure representations. All four models have the capacity to simulate full and zero structural flap-lag couplings of the experimental model. The lag-damping predictions are based on four aerodynamic theories, which range from linear (quasisteady) theory to a relatively comprehensive dynamic stall and wake theory. To simplify the subsequent presentation of results and clarify terminology, we briefly describe these four models of root-flexure-blade assembly and four aerodynamic theories.

2.1 Root-Flexure-Blade Assembly

2.1.1 Rigid Flap-Lag Model

It is an offset-hinged rigid blade with flap and lag (inplane) degrees of freedom; the flap and lag hinges are spring restrained and coincident (Ref. 2).

2.1.2 Spring Model

The root-flexure is simulated by a set of three linear springs located at an effective hinge offset; the spring stiffnesses are based on measured values. The airfoil or the blade portion has uniform mass and stiffness distributions. The bending-torsion couplings of the root spring system are fully accounted for (Ref. 3).

2.1.3 Modified Model

The root flexure is simulated by a short beam, over which the mass and stiffness properties are kept uniform. Their magnitudes are chosen so as to reasonably match the fundamental, nonrotating bending and torsion frequencies of the experimental model, and thus to those of the spring model. With judicious choice of hinge offset and the length of root beam it is possible to match the nonrotating and rotating frequencies of the first two flap-bending, lag-bending and torsional modes of the spring model (Ref. 3).

2.1.4 Modal Model

The actual mass and stiffness distributions of the root-flexure-blade assembly of the test model are used in calculating the nonrotating mode shapes numerically.

2.2 Aerodynamics

The aerodynamic representation called the dynamic stall and wake theory is fairly comprehensive. It includes the effects of dynamic stall lift, drag and pitching moment from a thin airfoil theory (Refs. 9 and 10) and the downwash effects from a finite-state three-dimensional wake theory (Ref. 11). Moreover, the airfoil theory includes the effects of reversed flow and

large angles of attack, and the wake theory accounts for the finite number of blades. We begin with a brief account of dynamic stall theory. This is followed by a mention of how quasisteady stall and linear theories are recovered as special cases. We conclude this section with a discussion of dynamic stall and wake theory.

2.2.1 Dynamic Stall Theory

It is based on the ONERA models of unified lift, drag and pitching moment. Basically we introduce lift circulation Γ, circulation-like drag Γ_d and circulation-like pitching moment Γ_m as follows:

$$\Gamma = \Gamma_1 + \Gamma_2,\ \Gamma_d = \Gamma_{d_1} + \Gamma_{d_2},\ \Gamma_m = \Gamma_{m_1} + \Gamma_{m_2} \tag{1}$$

where subscripts 1 and 2 indicate the linear and stalled or nonlinear components, respectively. These six components, two each in lift, drag and pitching moment are governed by Eqs. (2) - (4).

Dynamic Stall Lift:

$$k\dot{\Gamma}_1 + \lambda\Gamma_1 = \lambda a\left(U_y + b\dot{\varepsilon}\right)\cos\alpha + \delta b\dot{\varepsilon} \tag{2a}$$

$$\begin{aligned} k^2\ddot{\Gamma}_2 + 2dwk\dot{\Gamma}_2 + w^2\left(1+d^2\right)\Gamma_2 &= -w^2\left(1+d^2\right)\left[U\Delta C_z + ek\left(\dot{U}_x\cos\alpha + \dot{U}_y\sin\alpha\right)\Delta C_z\right. \\ &+ \left. ek\left(\dot{U}_y\sin\alpha - \dot{U}_x\cos\alpha\right)\frac{\partial\Delta C_z}{\partial\alpha}\right] \end{aligned} \tag{2b}$$

Dynamic Stall Drag:

$$\Gamma_{d_1} = UC_{d_0} \tag{3a}$$

$$k^2\ddot{\Gamma}_{d_2} + a_d k\dot{\Gamma}_{d_2} + r_d^2\Gamma_{d_2} = -\left[r_d^2 U\Delta C_d + E_d k\dot{U}_y\right] \tag{3b}$$

Dynamic Stall Pitching Moment:

$$\Gamma_{m_1} = UC_{m_0} + \delta_m b\dot{\varepsilon} \tag{4a}$$

$$k^2\ddot{\Gamma}_{m_2} + a_m k\dot{\Gamma}_{m_2} + r_m^2\Gamma_{m_2} = -\left[r_m^2 U\Delta C_m + E_m k\dot{U}_y\right] \tag{4b}$$

It is seen that the linear components in Eqs. (2a), (3a) and (4a) follow the classical thin airfoil theory. By comparison, the stalled components have an involved algebraic structure

and merit additional comments. For example, in Eqs. (2b), (3b) and (4b), $\Delta C_z, \Delta C_d$ and ΔC_m act like driving forces and represent the differences between the linear and quasisteady values of the airfoil section characteristics. For example, ΔC_z at an instantaneous angle of attack α is the difference between the extrapolated linear lift coefficient and the quasisteady stall lift coefficient of the airfoil; for details, see Ref. 12. Similarly, λ, δ, d, e and w in the lift equation; a_d, r_d and E_d in the drag equation and δ_m, a_m, r_m and E_m in the pitching-moment equation are determined on the basis of wind-tunnel experiments. Another important parameter in the linear part of the lift equation is $\dot{\varepsilon}$, which represents the airfoil rotation rate relative to airmass and includes complete geometric rotations of the airfoil.

It is expedient to represent the above airfoil lift Γ, drag Γ_d and pitching moment Γ_m in the local airfoil coordinates in terms of L_x, L_y and M as shown in Fig. 1. This is done in Eqs. (5a)-(5c).

$$L_y = U_x\left[\Gamma_1 + \Gamma_2\right] + U_y\left[\Gamma_{d_1} + \Gamma_{d_2}\right] + L_0 \tag{5a}$$

$$L_x = -U_y\left[\Gamma_1 + \Gamma_2\right] + U_x\left[\Gamma_{d_1} + \Gamma_{d_2}\right] \tag{5b}$$

$$M = 2b\left[U\left(\Gamma_{m_1} + \Gamma_{m_2}\right)\right] + M_0 \tag{5c}$$

where L_0 and M_0 are apparent mass lift normal to the chord and noncirculatory pitching moment at the three-quarter chord point.

2.2.2 Quasisteady Stall Theory

It includes the airfoil-section quasisteady stall characteristics. From Eqs. (2)-(4), by suppressing dynamic stall characteristics we get

$$\Gamma_1 = a\left(U_y + b\dot{\varepsilon}\right)\cos\alpha; \quad \Gamma_2 = -U\Delta C_z \tag{6a}$$

$$\Gamma_{d_1} = UC_{d_0}; \quad \Gamma_{d_2} = -U\Delta C_d \tag{6b}$$

$$\Gamma_{m_1} = UC_{m_0} + \delta_m b\dot{\varepsilon}; \quad \Gamma_{m_2} = -U\Delta C_m \tag{6c}$$

2.2.3 Linear Theory

Similarly, by suppressing the quasisteady stall characteristics the equations of lift, drag and pitching moment, including effects of reversed flow and large angles of attack, are:

$$\Gamma_1 = a\left(U_y + b\dot{\varepsilon}\right)\cos\alpha; \quad \Gamma_2 = 0 \tag{7a}$$

$$\Gamma_{d_1} = UC_{d_0}; \quad \Gamma_{d_2} = 0 \tag{7b}$$

$$\Gamma_{m_1} = UC_{m_0} + \delta_m b\dot{\varepsilon}; \quad \Gamma_{m_2} = 0 \tag{7c}$$

2.2.4 Dynamic Stall and Wake Theory

It is dynamic stall theory with downwash dynamics modeled by a finite-state three-dimensional wake theory due to Peters, Boyd and He (Ref. 11). At a blade station with radial coordinate $\overline{r}_i$ and spatial azimuth ψ_i, the instantaneous wake or downwash $\lambda\left(\overline{r}_i, \psi_i, t\right)$ is given by a complete set of radial shape functions $\phi_j^r\left(\overline{r}_i\right)$ and spatial harmonics $\cos(r\psi_i)$ and $\sin(r\psi_i)$:

$$\lambda\left(\overline{r}_i, \psi_i, t\right) = \sum_{r=0}^{\infty} \sum_{j=r+1,r+3}^{\infty} \phi_j^r\left(\overline{r}_i\right)\left[\alpha_j^r(t)\cos(r\psi_i) + \beta_j^r(t)\sin(r\psi_i)\right] \tag{8}$$

The cosine component $\alpha_j^r(t)$ and the sine component $\beta_j^r(t)$ are the dynamic states of the downwash and are governed by

$$\mathbf{M}\left\{\dot{\alpha}_j^r\right\} + \mathbf{V}\mathbf{L}_c^{-1}\left\{\alpha_j^r\right\} = 0.5\left\{\tau_n^{mc}\right\} \tag{9a}$$

$$\mathbf{M}\left\{\dot{\beta}_j^r\right\} + \mathbf{V}\mathbf{L}_s^{-1}\left\{\beta_j^r\right\} = 0.5\left\{\tau_n^{ms}\right\} \tag{9b}$$

where $\mathbf{V}$ is the diagonal matrix with $V_{11} = V_t = \sqrt{\left(\mu^2 + \lambda_t^2\right)}$ and all other elements are given by $V = \left[\mu^2 + \left(\lambda_t + \lambda_m\right)\lambda_t\right] / \sqrt{\left(\mu^2 + \lambda_t^2\right)}$. Closed-form expressions are available for the diagonal mass matrix $\mathbf{M}$ and influence coefficient matrices $\mathbf{L}_c$ and $\mathbf{L}_s$. Similarly, τ_n^{mc} and τ_n^{ms} are cosine and sine components of the pressure coefficient, which, for a rotor with Q blades, are given by

$$\tau_n^{0c} = \frac{1}{2\pi}\sum_{i=1}^{Q}\int_0^1 \frac{L_i\phi_n^0\left(\overline{r}_i\right)}{\rho\Omega^2R^3}d\overline{r}_i \tag{10a}$$

$$\tau_n^{mc} = \frac{1}{\pi}\sum_{i=1}^{Q}\int_0^1 \frac{L_i\phi_n^m\left(\overline{r}_i\right)}{\rho\Omega^2R^3}d\overline{r}_i\cos\left(m\psi_i\right) \tag{10b}$$

$$\tau_n^{ms} = \frac{1}{\pi}\sum_{i=1}^{Q}\int_0^1 \frac{L_i \phi_n^m(\bar{r}_i)}{\rho\Omega^2 R^3} d\bar{r}_i \sin(m\psi_i) \tag{10c}$$

A final comment concerns the computation of equilibrium-state inflow. In linear, quasi-steady stall, and dynamic stall theories it is computed from the momentum theory, while in the dynamic stall and wake theory it is computed from the coupled blade-wake-stall equations.

3 Analysis

For the rigid flap-lag model of the root-flexure-blade assembly, we follow Ref. 2 for the equations of motion including the hinge-offset effects. For the elastic blade models, the equations of flap bending, lag bending and torsion are based on Hamilton's principle with a second-order ordering scheme. The spatial dependence is treated by a Galerkin scheme using the uncoupled nonrotating mode shapes. Development of closed-form expressions of the mode shapes is a routine exercise for the cantilever-beam and spring models. However, for the modified model, we use the closed-form expressions developed in Ref. 3 using computer algebra; the mode shapes refer to a stepped beam with one end fixed and the other free. At the junction of the blade and the root flexure, there is discontinuity in the distributions of mass and flap-lag-torsion stiffnesses. The closed-form expressions account for this discontinuity and provide continuous displacements, slopes, moments and shear forces. For the modal model, the nonrotating modes are calculated by Myklestad-type and finite element schemes with mass and stiffness distributions identical to those of the experimental model. The modes from these two schemes agree. Moreover, we have also done extensive spot checks using the rotating mode shapes; trim and damping predictions from these two types of mode shapes agree. Throughout, the Galerkin-type integrals are calculated numerically.

As in the experimental rotor (Refs. 6 and 7), the analytical model in the correlation has three blades of the NACA 23012 airfoil section and, as detailed earlier, the root-flexure-blade assembly modeling varies from a simple offset-hinged rigid blade model to three different root-flexure models with elastic blades. In the convergence study on wake modeling and in the parametric study we consider an isolated rotor with three cantilever blades of the NACA

23012 airfoil section. To include dynamic stall lift, drag and pitching moment, the blade is discretized into five equal-length elements; each element has 7 dynamic stall states (3 in lift and 2 each in drag and pitching moment). The airfoil-section quasisteady stall and dynamic stall characteristics of lift, drag and pitching moment for a complete sweep of angle of attack ($-180^0 \leq \alpha \leq 180^0$) are as in Ref. 3. In the convergence and parametric studies, the trim analysis refers to computing the control inputs — collective pitch angle θ_0, longitudinal cyclic pitch angle θ_c, lateral cyclic pitch angle θ_s and shaft tilt angle α_s — and the corresponding periodic responses. The control inputs and the initial conditions for periodic response are computed simultaneously by periodic shooting. The resulting nonlinear equations are solved by a damped Newton iteration with a damping parameter of 0.7. Occasional divergence problems are encountered at high-thrust and high-advance-ratio conditions. Under such conditions, the results are obtained by either adjusting the Newton damping parameter or using a continuation approach with no damping; also see Ref. 13. The Floquet transition matrix for perturbations about periodic response comes out as a byproduct of periodic shooting, and its eigenanalysis gives the damping levels. All the structural and aerodynamic states are included in trim analysis as well as in eigenanalysis. In the correlation study, the collective pitch angle θ_0 and shaft tilt angle α_s are known control inputs and the trim analysis refers to computing the periodic responses.

4 Results

The results are presented in three parts: *i*) wake-modeling detail necessary for converged results of trim and damping; *ii*) parametric study of these results to variations in system parameters and *iii*) correlation of damping predictions with the database of Ref. 6. In the first two parts, we consider the rotor in propulsive or flight trim and include all multiblade lag modes. In the third part, the correlation covers nearly the entire database of some 2000 points on lag regressive-mode damping. Unless otherwise specified, the following baseline values are used in the first two parts: $Q = 3$; $\sigma = 0.05$; $a = 5.73$; $\gamma = 5.29$; $\omega_\beta = 1.15$; $\omega_\zeta = 0.7$; $\omega_\phi = 5.0$; $C_{d_0} = 0.0079$; $\overline{f} = 0.01$. In the third part, the test focuses on the forward-flight aspects of the stability problem. The rotor is operated untrimmed with an unrestricted tilt

of the tip-path plane. To cover the gist of the database, it becomes necessary to include samples of all typical cases tested. Accordingly, we include the following cases: collective pitch angle ($0^0 \leq \theta_0 \leq 6^0$), shaft angle ($8^0 \leq \alpha_s \leq 20^0$) and advance ratio ($0 \leq \mu \leq 0.55$). The rotor speed $\Omega = 1000$ rpm, corresponding to a rotating lead-lag frequency $\omega_\zeta = 0.61$ and flap frequency $\omega_\beta = 1.1$. The flap-lag structural coupling is zero; this refers to the database for which the collective pitch angle is set manually by changes to the angle of the blade relative to the root flexure. The thrust level is obtained as part of the trim analysis. Low-thrust conditions occur when both the collective pitch angle and advance ratio are low or when a high collective pitch angle offsets a high shaft angle. Similarly, high (negative) thrust conditions occur at a low collective pitch angle when both the advance ratio and shaft angle are high. Thus, the correlation covers near-zero- to high-thrust conditions for various combinations of shaft angle, collective pitch angle and advance ratio. For additional details see Refs. 2, 6 and 7.

4.1 Wake Modeling

We now come to wake modeling for converged results of control inputs, periodic responses and damping levels. This involves a judicious combination of the number of radial shape functions with each harmonic or S and the total number of harmonics or M; see Eq. (8). It is less sensitive to S per se, M being the more dominant parameter. Results (not shown) demonstrate that three radial shape functions with each harmonic are adequate, as was the case in Refs. 1 and 8, which are based on linear aerodynamics; that is, linear quasisteady theory with wake dynamics. Accordingly, with $S = 3$, we determine M. We compute the control inputs, periodic responses and corresponding damping levels for a preset value of M and then we increase M in increments of one till convergence to preset tolerance is obtained. For $C_T/\sigma_s = 0.075$ and $\mu = 0.3$, Figs. 2, and 3 show, respectively, the control inputs, and the damping levels. In particular, Fig. 2 shows all four control inputs — three blade pitch settings and shaft tilt. It is seen that $M = 9$ essentially gives converged trim results in that maximum error with respect to the results for $M = 12$ is less than 4%. Similarly, Fig. 3 shows the damping levels of all three multiblade lag modes. We observe an oscillatory convergence trend, particularly with respect to the cyclic regressive and progressive modes,

and $M = 9$ gives the same degree of convergence as that obtained for the control inputs in Fig. 2. In Figs. 2 and 3, the case with $M = 1$ merits special mention; it is a dynamic-inflow approximation and the results clearly show the inadequacy of this approximation. Similarly, convergence of control inputs, periodic responses and the corresponding damping levels are investigated for different values of C_T/σ_s and μ covering the flight regimes of conventional helicopters. Although convergence degrades with increasing C_T/σ_s and μ, the wake model with $S = 3$ and $M = 9$ (57 wake states) is adequate.

4.2 Parametric Study

Figures 4-10 show parametric-study results with an essentially converged wake model (57 wake states with $M = 9$ and $S = 3$). The results are based on four aerodynamic theories, which are identified in the figures. Figure 4 shows the periodic responses of all six modal components — two each in flap bending, lag bending and torsion; advance ratio $\mu = 0.3$ and thrust level $C_T/\sigma_s = 0.1$. Appreciable quantitative differences are seen among these theories. For example, the amplitudes of the first-lag (first-flap) modes are 0.00324 (0.00505), 0.00548 (0.006), and 0.00646 (0.00775) from the linear, quasisteady stall and dynamic stall theories, respectively. Compared to 0.009 (0.0076) from the dynamic stall and wake theory, the respective percentage errors are 64 (34), 39 (21) and 28 (2). The linear theory vis-a-vis the quasisteady stall theory shows the effects of nonlinear airfoil-section characteristics. Similarly, we observe appreciable effects of dynamic stall and dynamic wake by comparing, respectively, dynamic stall theory with the quasisteady stall theory and with the dynamic stall and wake theory. Figure 4 also shows that dynamic stall and dynamic wake bring in qualitative changes in the periodic responses of high-frequency (> 2/rev) modes. For example, dynamic stall theory and dynamic stall and wake theory predict 4/rev oscillations in the second flap mode and 5/rev oscillations in the first torsion mode. Thus, Fig. 4 demonstrates the necessity of including the effects of dynamic stall and wake in the prediction of periodic responses in trim analysis. These aerodynamic aspects are further investigated in Figs. 5-7 with respect to the four control inputs. The thrust level C_T/σ_s is 0.075 in Fig. 5 and 0.1 in Fig. 6 and the advance ratio μ varies from hover to 0.4 in both the figures. Figure 7 is a cross-plot of these two figures for varying thrust level at

$\mu = 0.4$. Overall, these three figures show that for $\mu < 0.4$ and at low-thrust conditions ($C_T/\sigma_s \leq 0.05$) all four theories are fairly close; this is expected. However, with increasing thrust level and advance ratio the dynamic stall and dynamic wake effects increase, and so do the differences among these theories. For example, at $\mu = 0.4$ and $C_T/\sigma_s = 0.1$ the longitudinal cyclic pitch θ_c is equal to 3^0 (or 0.05 rad) and 9^0 according to linear and quasisteady stall theories whereas it rapidly increases to 23^0 and 27^0 according to dynamic stall and dynamic stall and wake theories. This is because a major portion of the rotor disk is stalled under such high-thrust and high-advance ratio conditions; this demands high pitch settings to maintain the required thrust and moment conditions. Moreover, compared to the sensitivity of three pitch settings to dynamic stall and dynamic wake, the shaft tilt α_s is less sensitive. Overall, Figs. 5-7 show that the effects of dynamic stall and wake rapidly increase with increasing thrust level and advance ratio.

Figures 8-10 show the damping levels of the three multiblade lag modes; the three-bladed rotor is in propulsive trim and the predictions are based on the four aerodynamic theories referred to earlier. The thrust level $C_T/\sigma_s = 0.075$ in Fig. 8 and it increases to 0.1 in Fig. 9. Figure 10 is a sort of cross-plot of Figs. 8 and 9 at a relatively high advance ratio of 0.4, and it includes additional damping results for a thrust level of 0.05. As seen from Fig. 8, the quasisteady stall theory deviates appreciably from the linear theory; by contrast it is closer to the other two theories: dynamic stall, and dynamic stall and wake theories. This deviation is due to nonlinear airfoil characteristics of substall drag and quasisteady stall lift and drag. The effects of quasisteady stall pitching moment are negligible. At low advance ratios, the substall drag dominates, and with increasing advance ratio the effects of quasisteady stall lift and drag become increasingly important in the quasisteady stall theory. Up to an advance ratio of 0.25 or so, the quasisteady stall theory agrees with the dynamic stall theory and to some extent with the dynamic wake and stall theory as well. From hover to an advance ratio of 0.1, dynamic stall and wake theory predicts less damping for the regressive and progressive modes owing to downwash effects. For advance ratio $\mu \geq 0.25$, the quasisteady stall theory consistently underpredicts damping, and this underprediction increases with increasing advance ratio owing to increasing dynamic stall effects; the minor differences between the dynamic stall and dynamic stall and wake

theories are due to downwash dynamics. Figure 9 is basically a magnified version of Fig. 8, particularly regarding the effects of dynamic stall and wake with increasing thrust level. The regressive mode damping, in particular, shows that dynamic wake effects are appreciable for practically all advance ratios ($0 \leq \mu \leq 0.4$). A comparison between the quasisteady stall and dynamic stall theories shows that for $\mu > 0.2$ dynamic stall effects rapidly increase with increasing advance ratio. Figure 10 is more or less a summary of Figs. 8 and 9, although for a fixed value of μ. Even at low-thrust levels ($C_T/\sigma_s \leq 0.05$) the inadequacy of the linear theory in predicting lag damping is clearly seen and as expected, the other three theories agree well. By comparing dynamic stall theory, respectively, with the quasisteady stall theory and with the dynamic stall and wake theory, Fig. 10 shows that the effects of dynamic stall and wake increase with increasing thrust level. Overall, Figs. 8-10 demonstrate the necessity of including dynamic stall and wake in predicting damping levels.

4.3 Correlation

We reiterate that the damping levels are generated from four structural models of the root-flexure-blade assembly and that the predictions from each structural model are based on the four aerodynamic theories referred to earlier. With such a wide range of structural and aerodynamic representations, we bracket the extent of the sensitivity of the predictions to structural approximations and thereby isolate the aerodynamic aspects of the delicate lag-damping predictions without allowing the correlation to be overly masked by this sensitivity. The computer time for such comprehensive predictions covering nearly 2000 test points of the database on lag-regressive mode damping is nearly prohibitive. To somewhat minimize this constraint, the correlation uses a wake model with $S = 3$ and $M = 7$ (not 9 as done in Figs. 2-10) and the maximum error compared to the results with $S = 3$ and $M = 9$ is less than 12%. In Figs. 11-13 we present the correlation based on the modified model, and then in Figs. 14-16 we compare the predictions from the four structural models of the root-flexure-blade assembly using the dynamic stall and wake theory.

Figures 11a–11d show correlation for $\theta_0 = 0^0$ at high shaft angles; $\alpha_s = 12^0, 14^0, 16^0$ and 20^0, respectively. As seen from the data, the damping remains nearly constant from hover to an advance ratio of $\mu \approx 0.2$ and then increases sharply beyond $\mu = 0.3$. From

hover to an advance ratio of 0.1, owing to very low-thrust conditions, the predictions from all four aerodynamic theories are virtually identical. For $\mu > 0.3$, some of the theories differ qualitatively. This result is expected; for the present combination of low collective pitch and high shaft tilt angles, as the advance ratio increases, (negative) thrust level increases and thereby dynamic stall dominates. Basically, the linear theory predicts that damping increases slowly, and thereafter it significantly deviates from the data, leveling off and decreasing sharply. It is this sharp decrease that is not supported by the data. While this decrease occurs within the data-range for shaft angles 12^0 and 14^0, it occurs outside the data-range for shaft angles 16^0 and 20^0. The quasisteady stall theory shows sharply decreasing damping for $0.35 \leq \mu \leq 0.45$ at $\alpha_s = 12^0$ and 14^0, and for $0.3 \leq \mu \leq 0.4$ at $\alpha_s = 16^0$ and 20^0, and thereafter it shows rapidly increasing damping. The increase is so delayed that it makes the quasisteady stall theory unacceptable. In contrast, we have the dynamic stall, and dynamic stall and wake theories. For example, inclusion of dynamic stall dramatically improves the correlation. The dynamic stall theory follows the quasisteady stall theory till $\mu \approx 0.3$, and for $\mu > 0.3$ the dynamic stall effects dominate. In other words, for $\mu > 0.3$, the dynamic stall theory deviates remarkably from the quasisteady stall theory and improves the correlation. The inclusion of three-dimensional wake effects in addition to stall effects brings in further improvement. Overall, the dynamic stall, and dynamic stall and wake theories predict the trend of the data; that is, the damping basically increases with increasing advance ratio, although it is accompanied by localized humps and troughs.

Figure 12 shows the correlation for $\theta_0 = 3^0$. In Fig. 12a, $\alpha_s = 8^0$ and in Fig. 12b, $\alpha_s = 16^0$; the data are available for $0 \leq \mu \leq 0.25$ and for $0 \leq \mu \leq 0.35$, respectively. In Fig. 12a, the thrust level is relatively low throughout ($C_T/\sigma_s \leq 0.04$). It is about 0.03 in hover, and increases to 0.04 at $\mu = 0.1$ and thereafter continuously decreases with increasing advance ratio, down to nearly zero at $\mu \approx 0.55$. This is well reflected by the good correlation of the linear theory and closeness of the quasisteady stall and dynamic stall theories. Though the quasisteady stall and dynamic stall theories overpredict damping, they predict the trend of the data of nearly constant damping for the entire advance ratio range ($0 \leq \mu \leq 0.25$). The dynamic stall and wake theory falls in between the linear theory, and the quasisteady stall and dynamic stall theories. It improves the correlation by significantly

reducing the overprediction of the quasisteady stall and dynamic stall theories and thus provides satisfactory correlation throughout.

The data in Fig. 12b show clearly the trend of decreasing damping with increasing advance ratio. The thrust level, which is about 0.03 in hover, changes to -0.05 at $\mu = 0.35$. The linear theory predicts that the damping consistently increases with increasing advance ratio, a trend opposite to that of the data. However, for $\mu > 0.5$ it predicts the trend of decreasing damping with increasing advance ratio ; but this decrease occurs far beyond the data range to be adequate. The quasisteady stall and dynamic stall theories come close to predicting the trend of the data for $0 \leq \mu \leq 0.25$, although the damping levels are overpredicted owing to nonlinear substall drag effects. The dynamic stall and wake theory shows improvement over the other three theories; still it falls short of predicting clearly the trend of the data within the data range. Given the very low thrust condition, neither dynamic stall nor dynamic wake is a major factor, and the required improvements merit further study.

Now, we present the correlation for $\theta_0 = 6^0$ and $\alpha_s = 20^0$ in Fig. 13. The linear theory shows that damping increases with increasing advance ratio from hover to $\mu = 0.45$ followed by a sharp decrease for $\mu \geq 0.5$. This is opposite to the trend of the data, which, though limited to very low advance ratios ($0 \leq \mu \leq 0.15$), show that damping very slowly decreases with increasing advance ratio. The quasisteady stall and dynamic stall theories predict the trend of the data despite appreciable overpredictions. The dynamic stall and wake theory significantly reduces these overpredictions and provides good correlation over the data range. The nonlinear substall drag accounts for much of the differences between the linear and quasisteady stall theories; this is a consequence of low-Reynolds-number effects of the test conditions. Dynamic stall is not an issue here, and unsteady lift effects account for the differences between the dynamic stall and quasisteady stall theories. Similarly, the effects of downwash account for the differences between the dynamic stall, and dynamic stall and wake theories.

4.3.1 Comparison of Structural Models

The preceding correlations based on the modified model (Figs. 11−13) and additional correlations based on other structural models (see Ref. 14) of the root-flexure-blade assembly show that the dynamic stall and wake theory is the best of the four aerodynamic theories. Given this background, we present in Figs. 14−16 a comparative assessment of four structural models based on the dynamic stall and wake theory. Figures 14a−14d show the effects of structural modeling for $\theta_0 = 0^0$ and $\alpha_s = 12^0, 14^0, 16^0$ and 20^0. To set the stage, we mention that with increasing advance ratio and shaft angle, the negative thrust level increases, as do the effects of dynamic stall. This brings in increased system nonlinearity, and accordingly damping predictions show increasing sensitivity to changes in blade modeling. This sensitivity is more clearly seen in Figs. 14c and 14d, for $\alpha_s = 16^0$ and 20^0, respectively. For shaft angles 12^0 and 14^0, the predictions from three elastic models are close and provide adequate correlation throughout. The rigid flap-lag model also provides satisfactory correlation up to an advance ratio of $\mu \approx 0.3$. The difference between the predictions from three elastic blade models and those from the rigid blade model is due to blade torsion and bending effects (Ref. 3). Overall, Figs. 14a-14d show that all the elastic blade models adequately predict the trend of the data.

Figure 15a for $\theta_0 = 3^0$ and $\alpha_s = 8^0$ shows that all four blade models give good correlations and that the spring model slightly overpredicts damping. This overprediction, though not appreciable quantitatively, is consistently observed throughout the data range. In Fig. 15b ($\theta_0 = 3^0$ and $\alpha_s = 16^0$) none of the blade models predict the trend of the data of decreasing damping with increasing advance ratio for the entire data range ($0 \leq \mu \leq 0.35$). All the models except the spring model provide adequate correlation for $\mu < 0.2$ or so. Finally, we come to Fig. 16 for $\theta_0 = 6^0$ and $\alpha_s = 20^0$, in which the data are limited to low advance ratios ($0 \leq \mu \leq 0.15$). It is seen that the modified model and the modal model provide good correlations. The predictions from the rigid flap-lag model are also adequate. The trend of the data is predicted by the spring model, but it consistently overpredicts damping. This overprediction is due to the overestimation of root-flexure bending-torsion coupling by the spring model, and it increases with increasing blade pitch; for example, compare Fig. 15a

and 15b with Fig. 16 at $\mu = 0$.

5 Concluding Remarks

The preceding wake modeling, parametric and correlation studies show that dynamic stall and wake effects are appreciable on control inputs, periodic responses and damping levels and lead to the following findings:

1. The dynamic wake model with nine harmonics ($M = 9$) and with three radial shape functions per harmonic gives essentially converged results in the presence of dynamic stall.

2. The effects of dynamic stall and dynamic wake on the control inputs, periodic responses and on the damping levels increase with increasing thrust level and advance ratio.

3. For nearly the entire database, the rigid flap-lag, modified and modal models provide adequate correlation. The predictions from the modified and modal models are nearly the same and run fairly close to the predictions from the rigid flap-lag model. However, with increasing negative thrust levels, as is the case for combinations of high advance ratio and high shaft angle at $\theta_0 = 0^0$, the modified and modal models provide better correlations.

4. For a set of data points at $\theta_0 = 3^0$ and high shaft angles the trend of the data of decreasing damping with increasing advance ratio is not well-predicted. This occurs at relatively low-thrust conditions and dynamic stall is not a major factor. Investigation is continuing.

5. For $\theta_0 = 0^0$ and high shaft angles, as the advance ratio increases, the effects of negatively stalled conditions increase. Under such conditions the predictions show increasing sensitivity to changes in modeling the root-flexure-blade assembly. Consequently, the differences in the predictions from four structural models increase with increasing negative thrust conditions.

6. The spring model also provides fairly adequate correlation for the entire database. But it overestimates the bending-torsion couplings of the root flexure. This overestimation brings in increasing quantitative degradation to the correlation with increasing blade pitch angle θ_0.

7. The dynamic stall theory is keyed to the airfoil-section characteristics of lift, drag and pitching moment under quasisteady-stall and dynamic-stall conditions. Improved representation of these characteristics under the low-Reynolds-number conditions of the experiment merits further research; this offers considerable promise in further improving the correlation.

6 Bibliography

1. Manjunath, A. R., Nagabhushanam, J., Gaonkar, G. H., Peters, D. A. and Su, A., "Flap-Lag Damping in Hover and Forward Flight With a Three-Dimensional Wake," *Journal of the American Helicopter Society*, Vol. 38, (4), Oct 1993.

2. Barwey, D., Gaonkar, G. H. and Ormiston, R. A., "Investigation of Dynamic Stall Effects on Isolated Rotor Flap-Lag Stability with Experimental Correlation," *Journal of the American Helicopter Society*, Vol. 36, (4), Oct 1991.

3. Barwey, D. and Gaonkar, G. H., "Dynamic-Stall and Structural-Modeling Effects on Helicopter Blade Stability with Experimental Correlation," *AIAA Journal*, Vol. 32, (4), Apr 1994.

4. Torok, M. S. and Chopra, I., "Hingeless Rotor Aeroelastic Stability Analysis With Refined Aerodynamic Modeling," *Journal of the American Helicopter Society*, Vol. 36, (4), Oct 1991.

5. Peters, D. A. and Su, A., "The Effect of Hidden Dynamic States of Floquet Eigenvalues," *Journal of the American Helicopter Society*, Vol. 35, (4), Oct 1990.

6. McNulty, M. J., "Flap-Lag Stability Data for a Small Scale Isolated Hingeless Rotor in Forward Flight," NASA TM 102189, Apr 1989.

7. Gaonkar, G. H., McNulty, M. J. and Nagabhushanam, J., "An Experimental and Analytical Investigation of Isolated Rotor Flap-Lag Stability in Forward Flight," *Journal of the American Helicopter Society*, Vol. 35, (2), May 1990.

8. Manjunath, A. R., Nagabhushanam, J., Gaonkar, G. H., Chunduru, Srinivas and Prasad Sampath, "Flap-Lag-Torsion Stability in Hover and Forward Flight With a Three-Dimensional Wake," Proceedings of the NASA-Ames/American Helicopter Society Aeromechanics Specialists Conference, San Francisco, CA, Jan 18-21, 1994.

9. Peters, D. A., "Toward a Unified Lift Model for Use in Rotor Blade Stability Analysis," *Journal of the American Helicopter Society*, Vol. 30, (3), Jul 1985.

10. Petot, D., "Differential Equation Modeling of Dynamic Stall," ONERA, Technical Note No. 5, 1989.

11. Peters, D. A., Boyd, D. D. and He, C. J., "Finite-State Induced-Flow Model for Rotors in Hover and Forward Flight," *Journal of the American Helicopter Society*, Vol. 34, (4), Oct 1989.

12. Barwey, D., "Dynamic Stall Effects on Hingeless Rotor Stability With Experimental Correlation," Ph.D. dissertation, College of Engineering, Florida Atlantic University, Boca Raton, FL, Apr 1992.

13. Achar, N. S. and Gaonkar, G. H., "Helicopter Trim Analysis by Shooting and Finite Element Methods with Optimally Damped Newton Iterations," *AIAA Journal*, Vol. 31, (2), Feb 1993.

14. Subramanian, S., Srinivas Chunduru, and Gaonkar, G. H., "Effects of Dynamic Stall and Three-Dimensional Wake Effects on Aeroelastic Stability of Isolated Hingeless Rotors with Experimental Correlation," Proceedings of the 50th Annual Forum of the American Helicopter Society, Washington, DC, May 11-13, 1994.

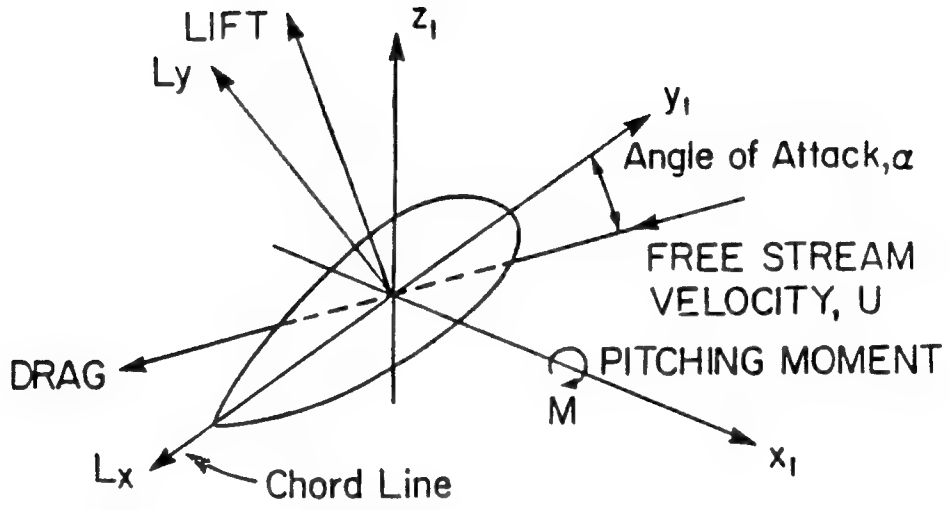

Figure 1: Schematic of Blade Section Aerodynamics

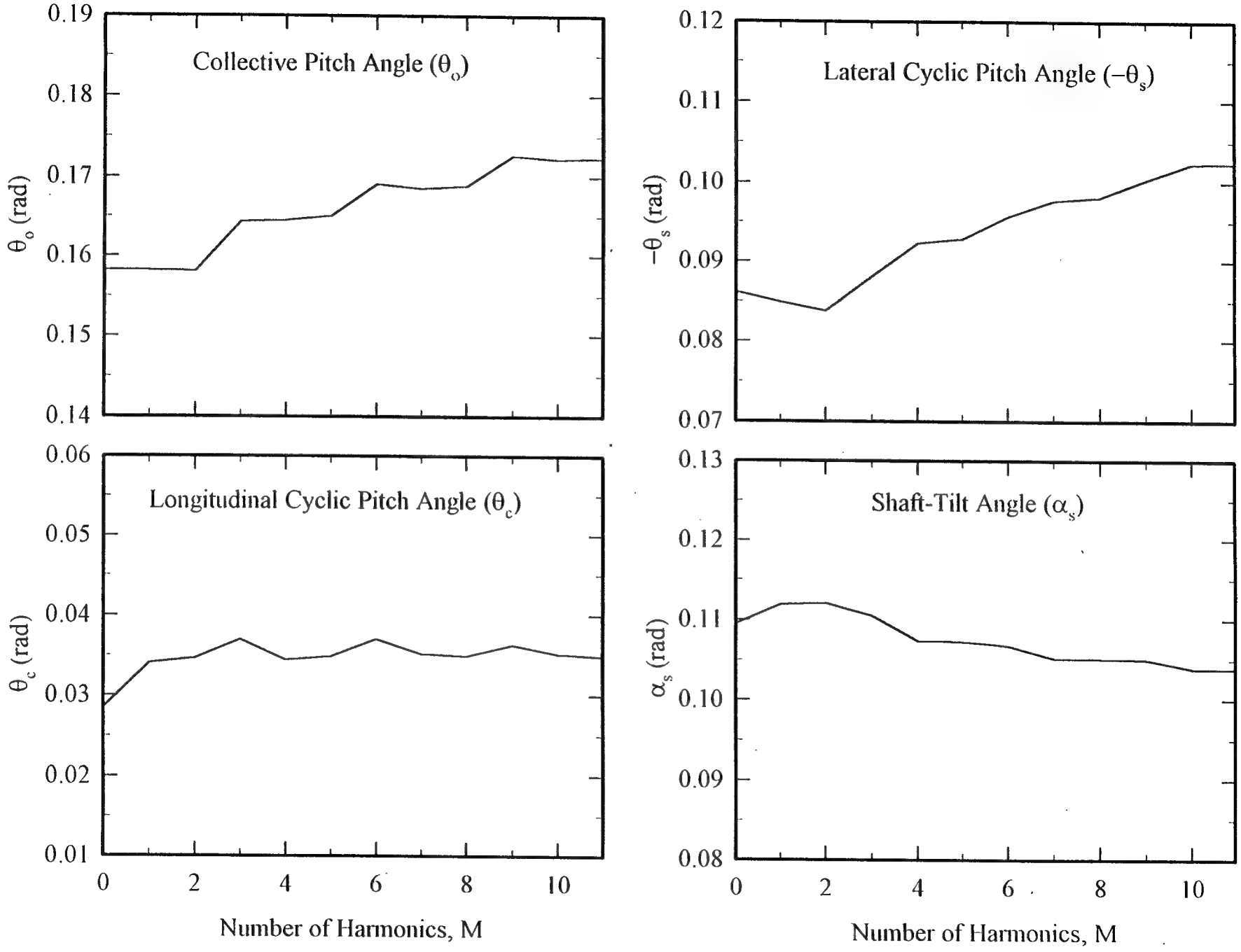

Figure 2: Convergence Trends of Trim Settings with Respect to Number of Harmonics for $\mu = 0.3$ and $C_T/\sigma_c = 0.075$.

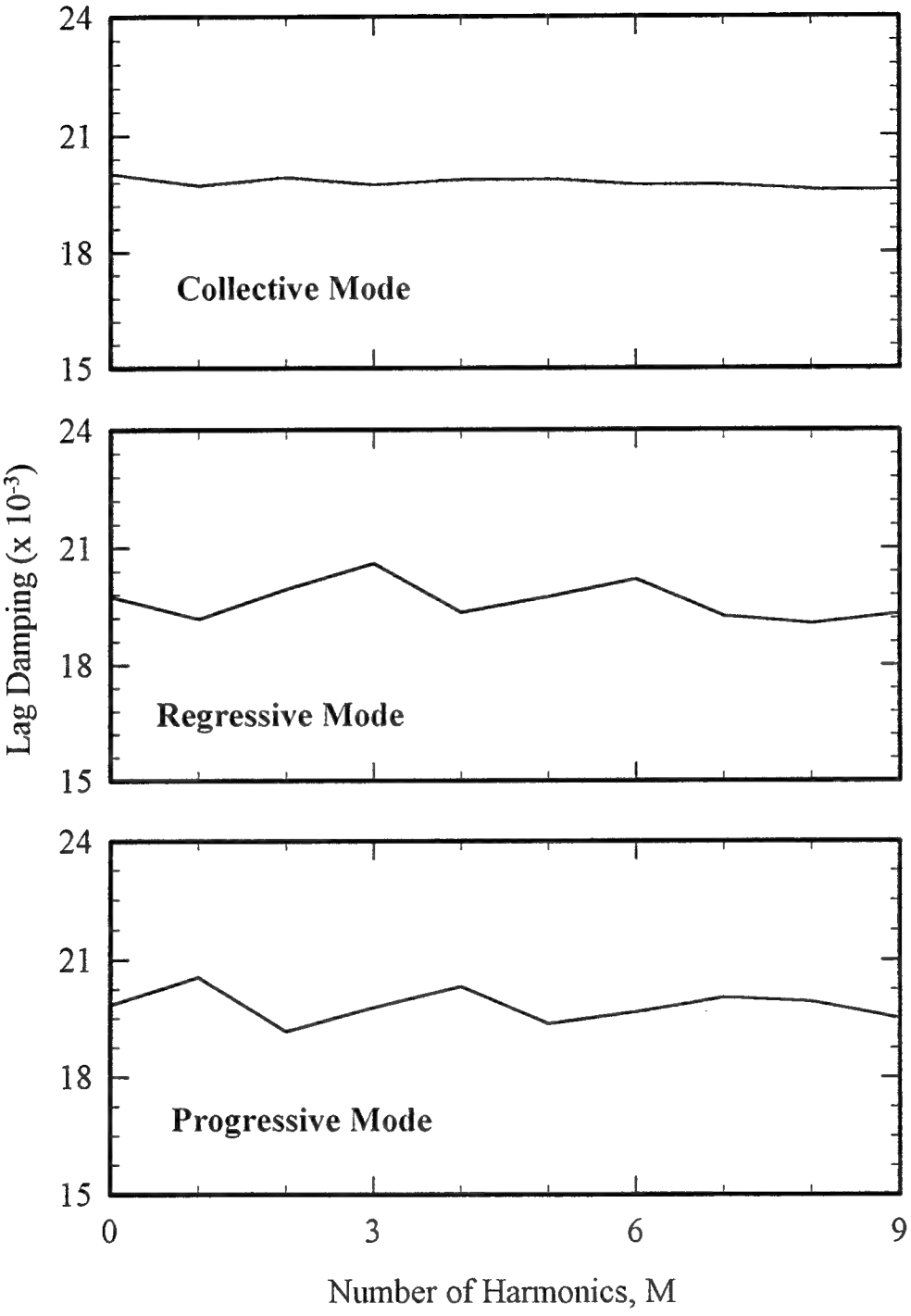

Figure 3: Oscillatory Convergence Trends of First Lag-Mode Damping Levels with Respect to Number of Harmonics for $\mu = 0.3$ and $C_T/\sigma_s = 0.075$.

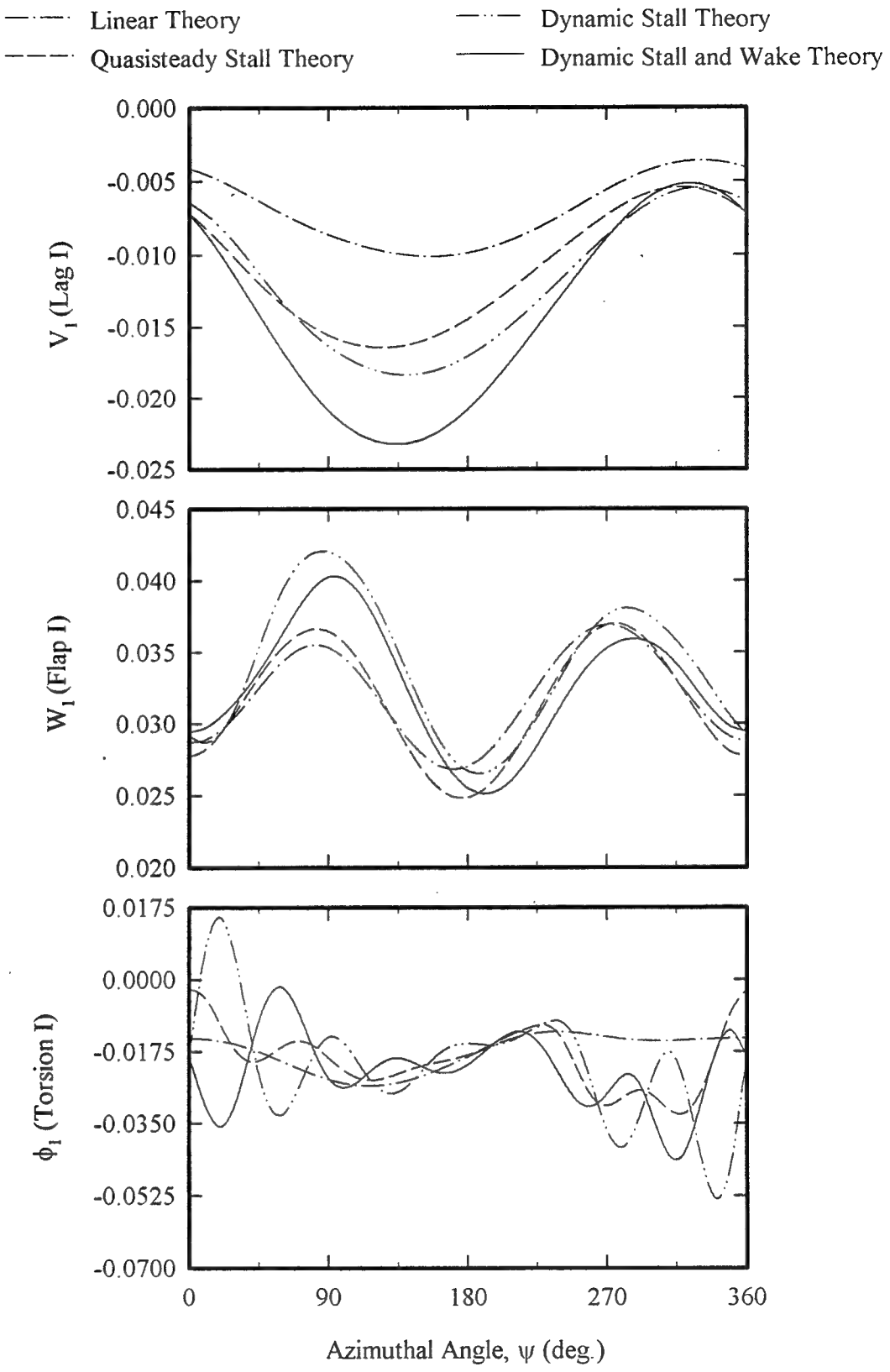

Figure 4: Effects of Aerodynamic Modeling on Periodic Responses for $\mu = 0.3$ and $C_T/\sigma_s = 0.1$. (concluded in the next page)

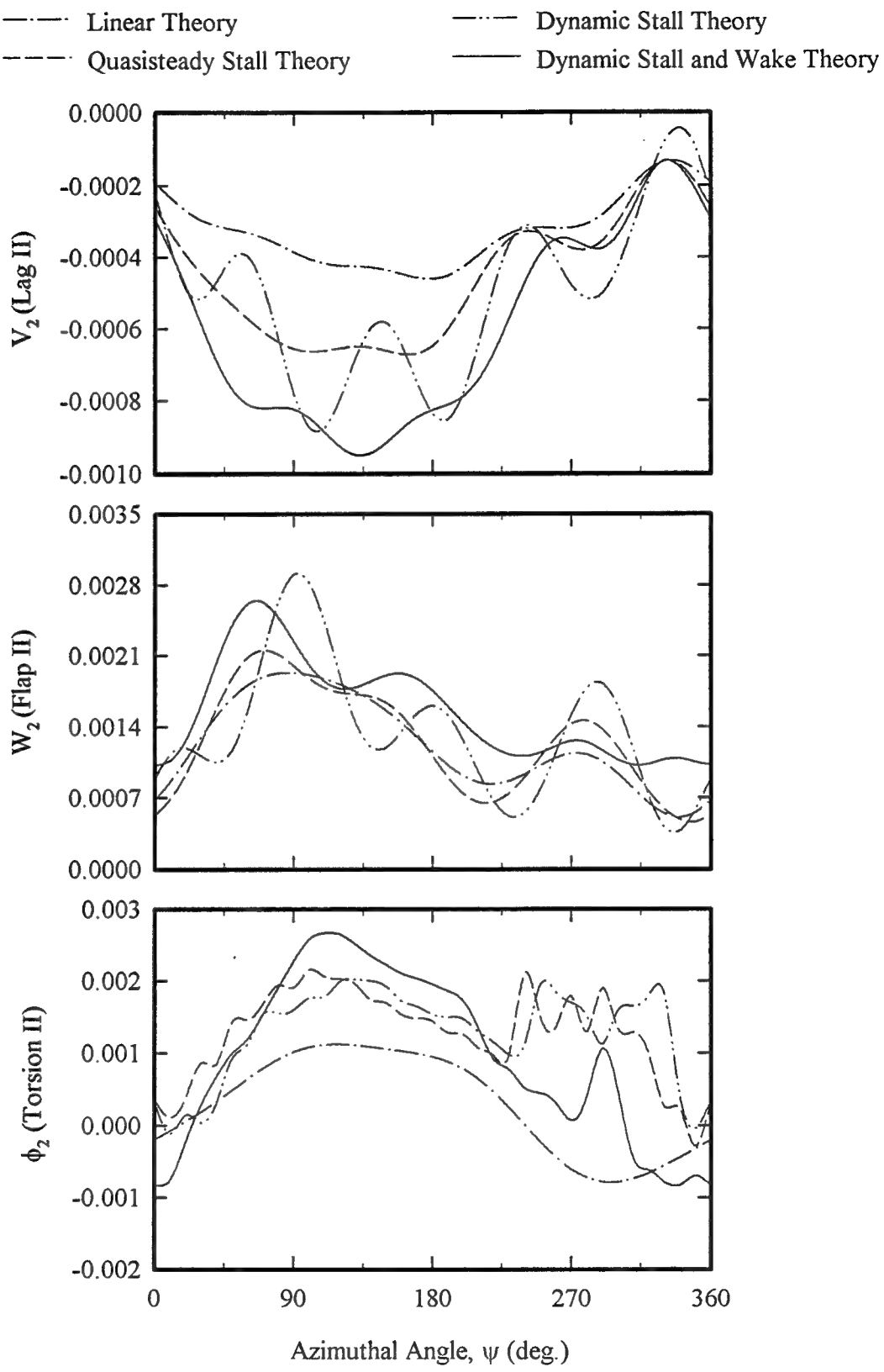

Figure 4 (continued): Effects of Aerodynamic Modeling on Periodic Responses for $\mu = 0.3$ and $C_T/\sigma_s = 0.1$.

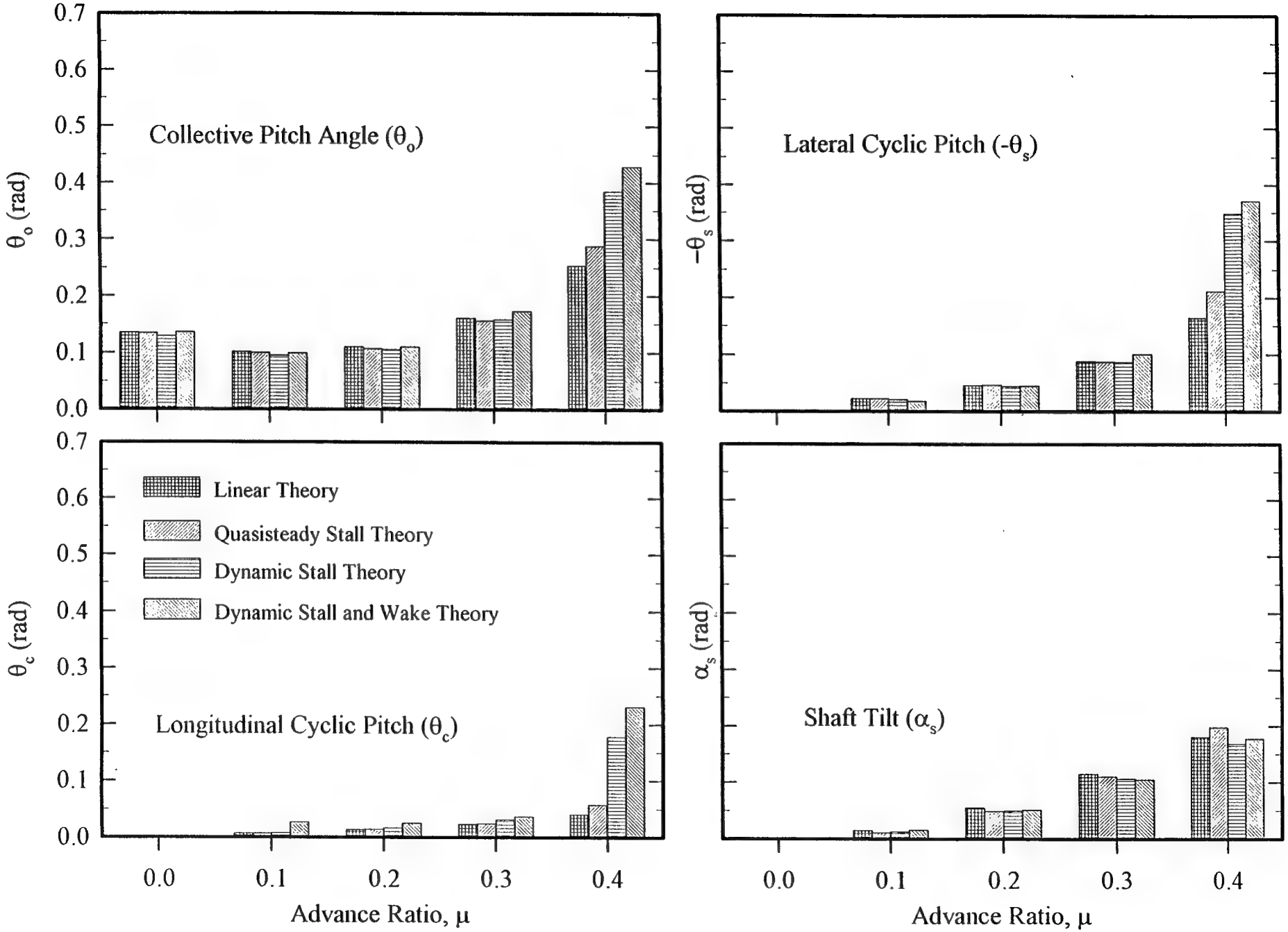

Figure 5: Effects of Aerodynamic Modeling on Control Inputs from Hover to Forward Flight for $C_T/\sigma_s = 0.075$.

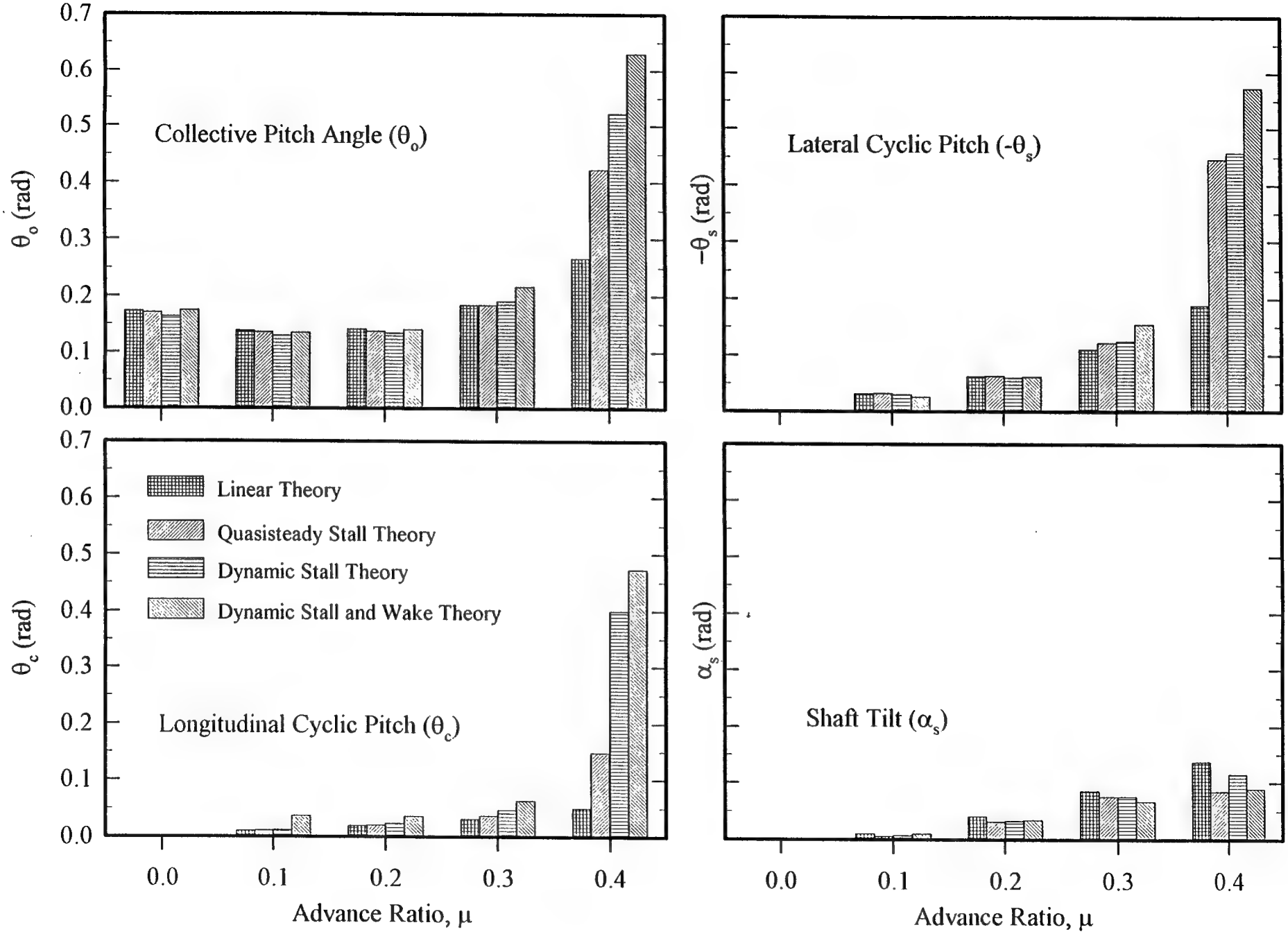

Figure 6: Effects of Aerodynamic Modeling on Control Inputs from Hover to Forward Flight for $C_T/\sigma_s = 0.1$.

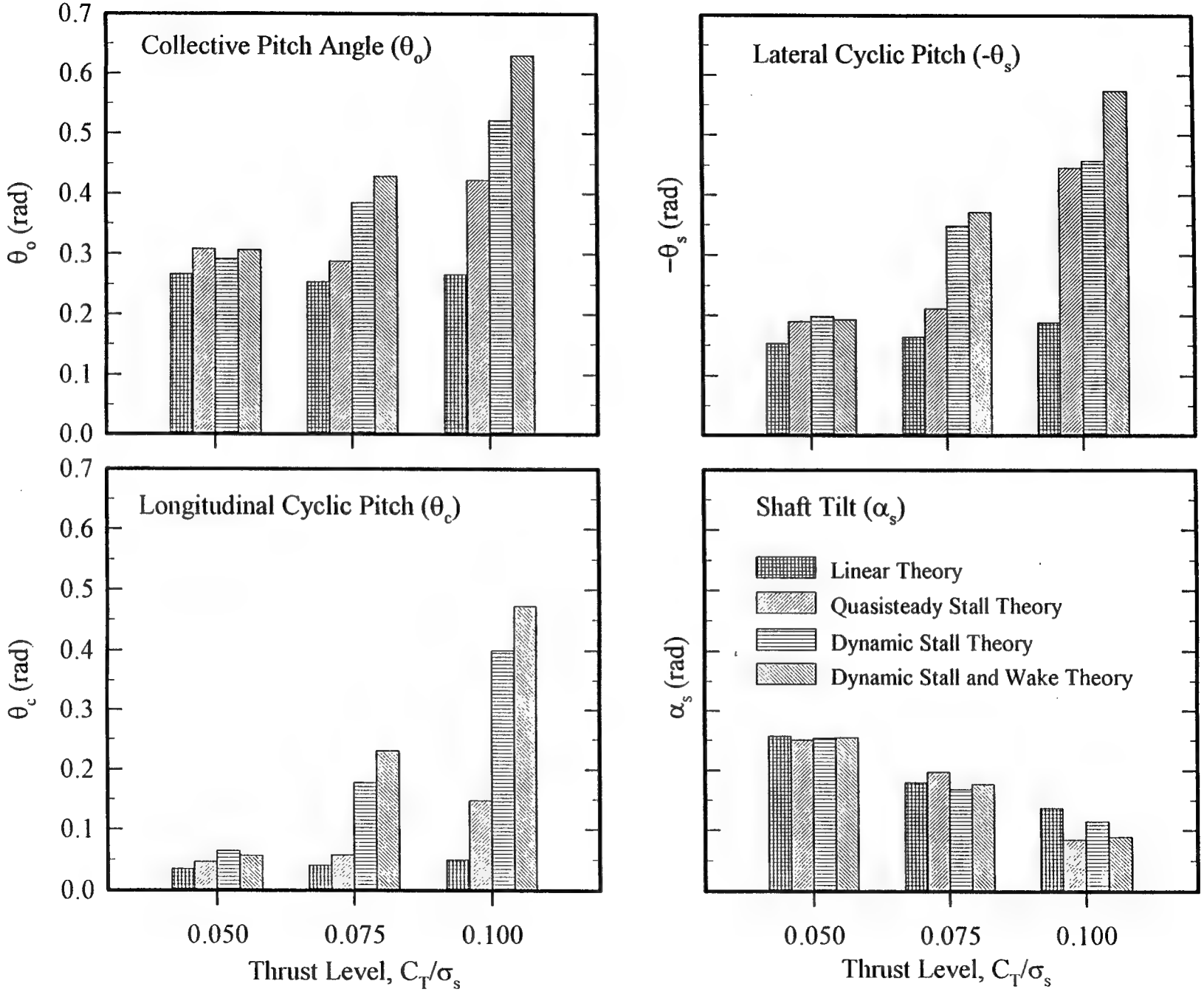

Figure 7: Control Inputs Vs. Thrust Level from Various Aerodynamic Theories for $\mu = 0.4$.

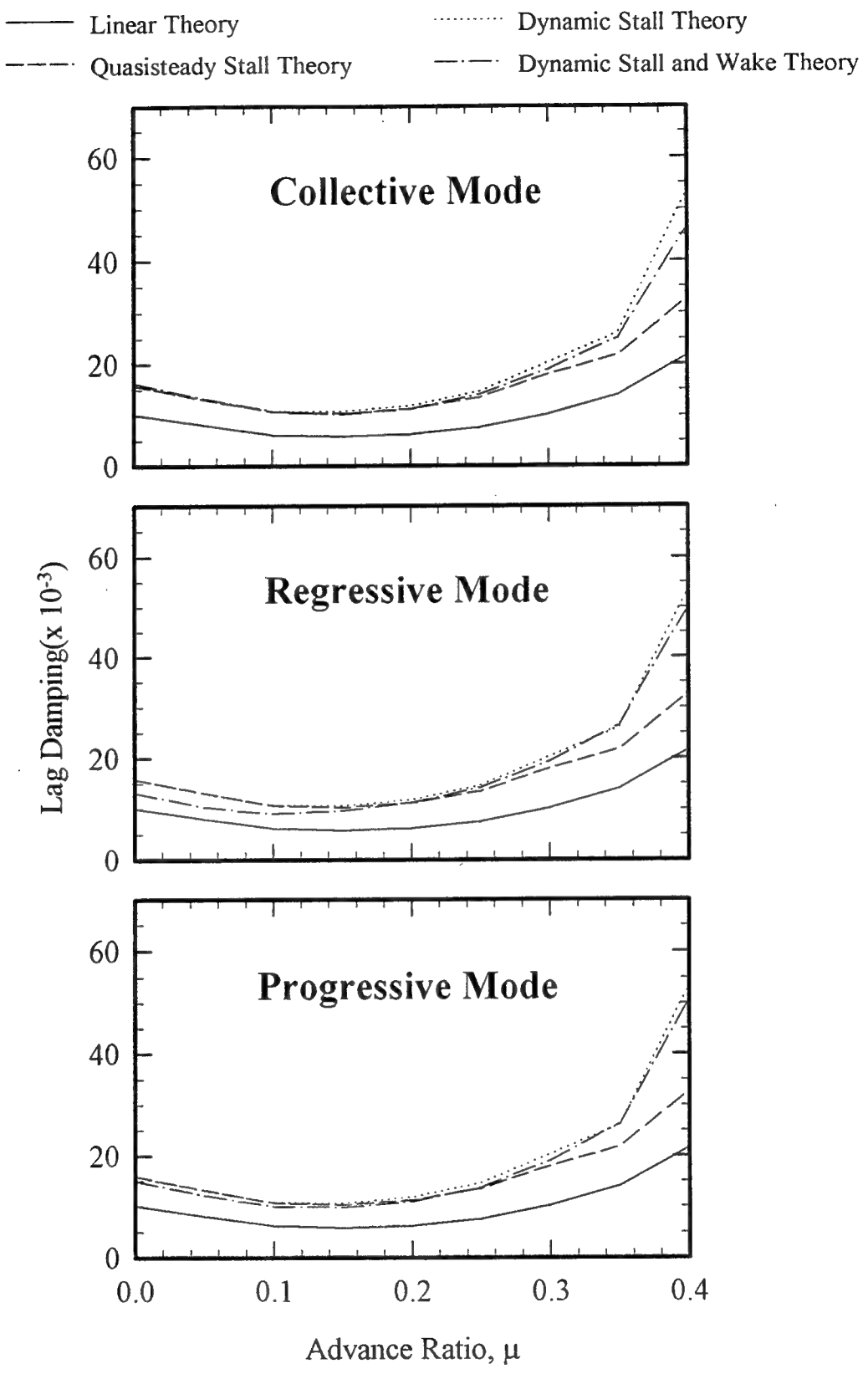

Figure 8: Effects of Aerodynamic Modeling on Lag-Damping Predictions from Hover to Forward Flight for $C_T/\sigma_s = 0.075$.

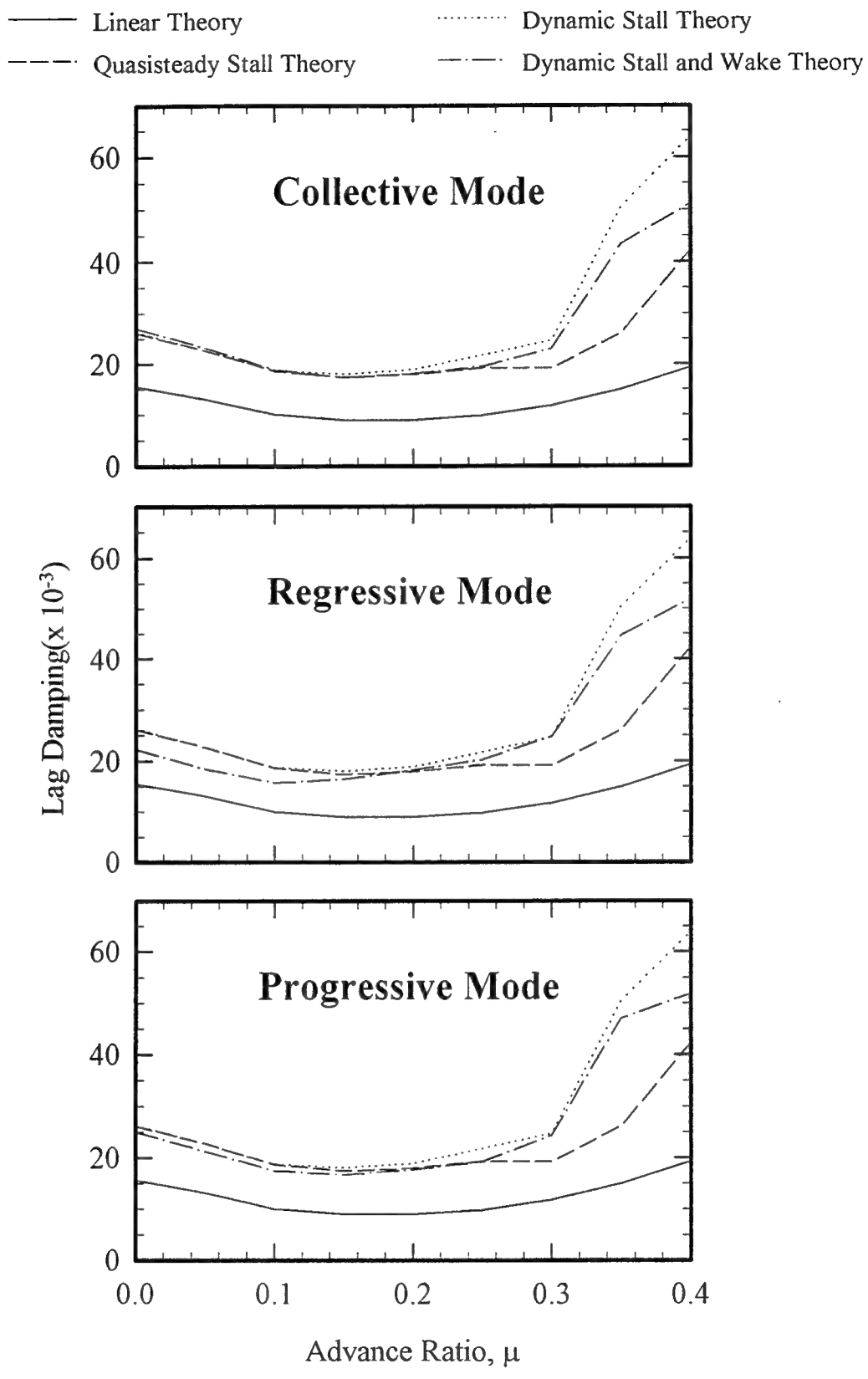

Figure 9: Effects of Aerodynamic Modeling on Lag-Damping Predictions from Hover to Forward Flight for $C_T/\sigma_s = 0.1$.

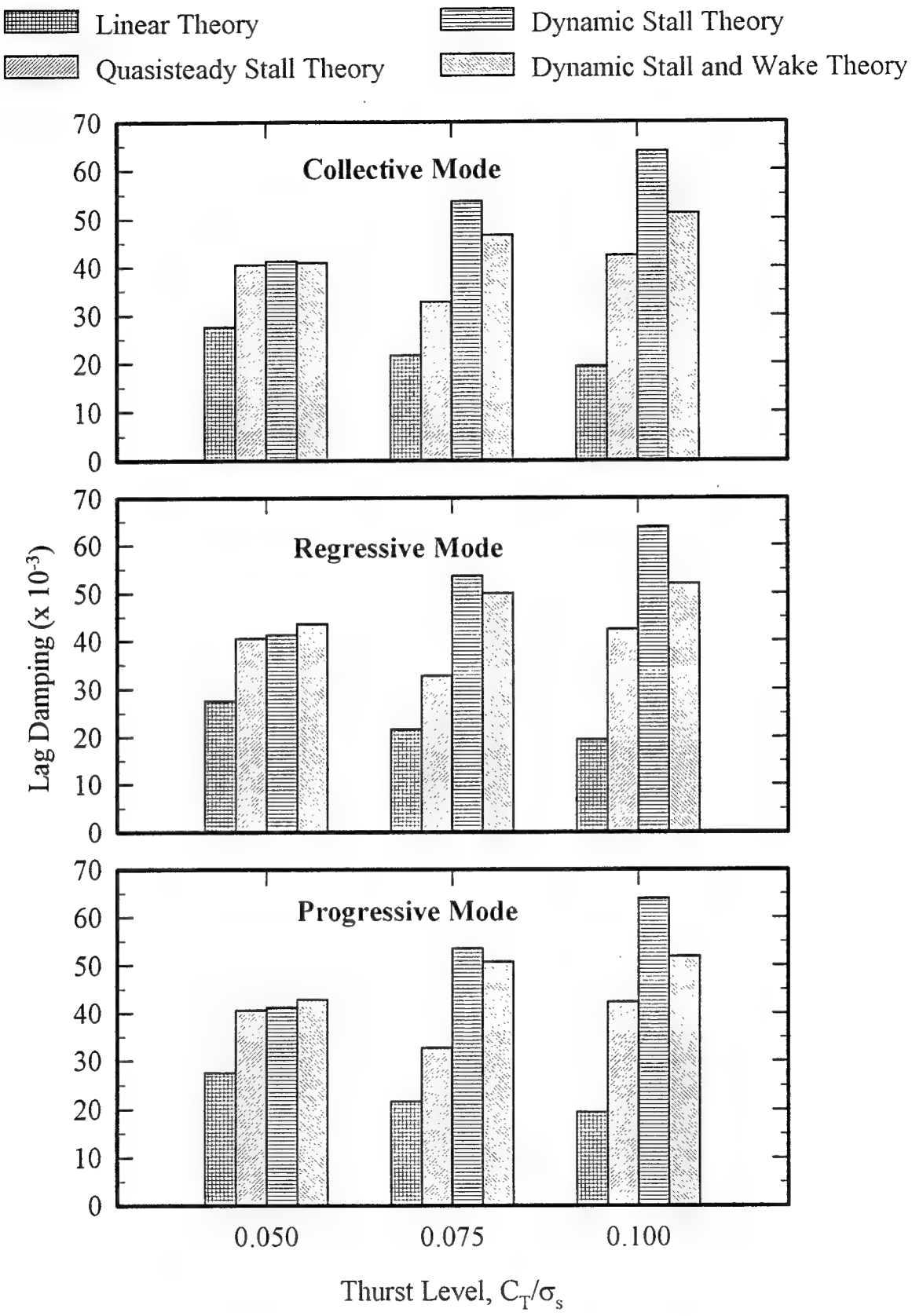

Figure 10: Lag-Damping Vs. Thrust Level from Various Aerodynamic Theories for $\mu = 0.4$.

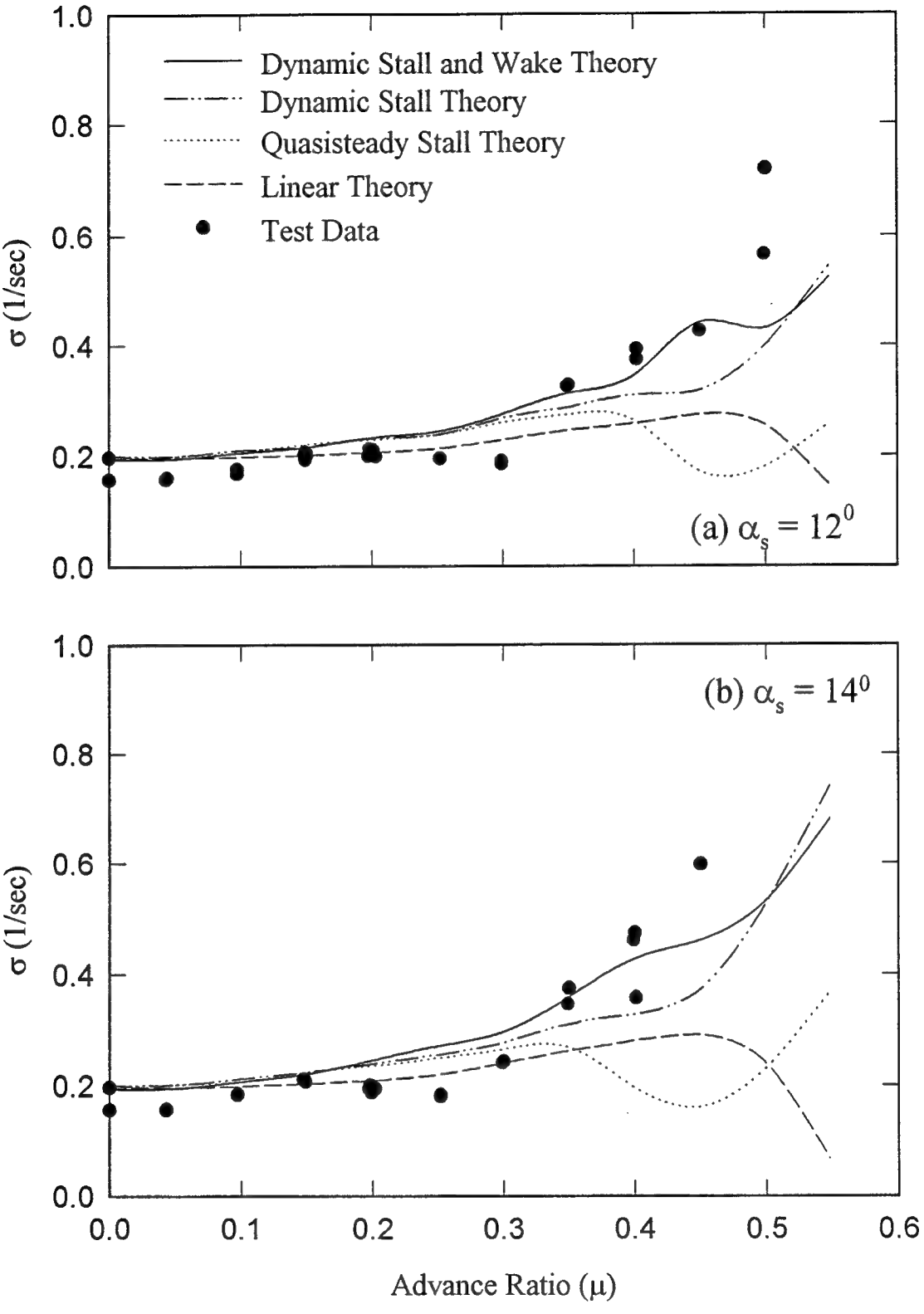

Figure 11: Effects of Aerodynamic Modeling on Lag-Damping Correlation from Modified Model for $\theta_0 = 0^0$ (concluded in the next page).

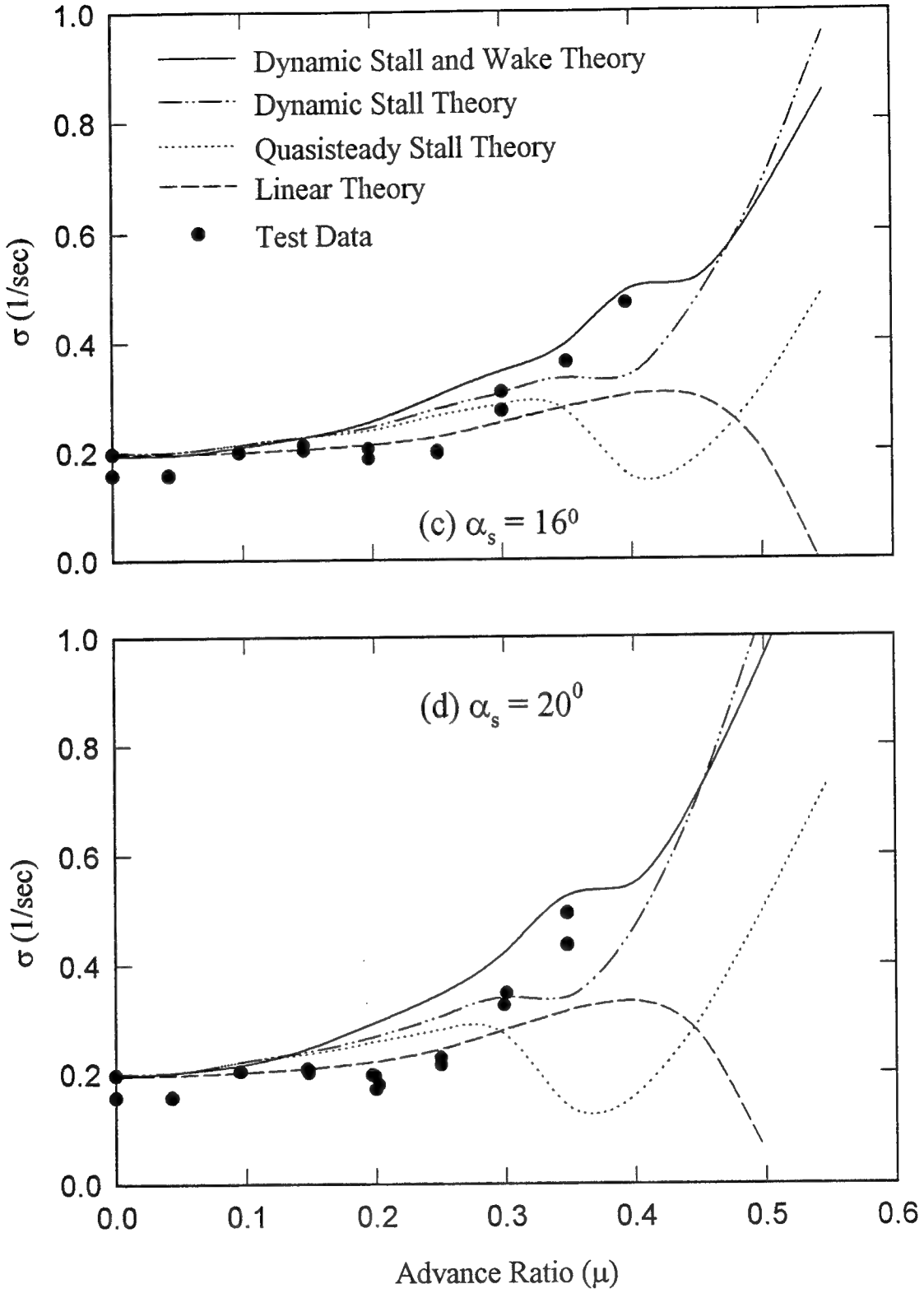

Figure 11 (continued): Effects of Aerodynamic Modeling on Lag-Damping Correlation from Modified Model for $\theta_0 = 0^0$.

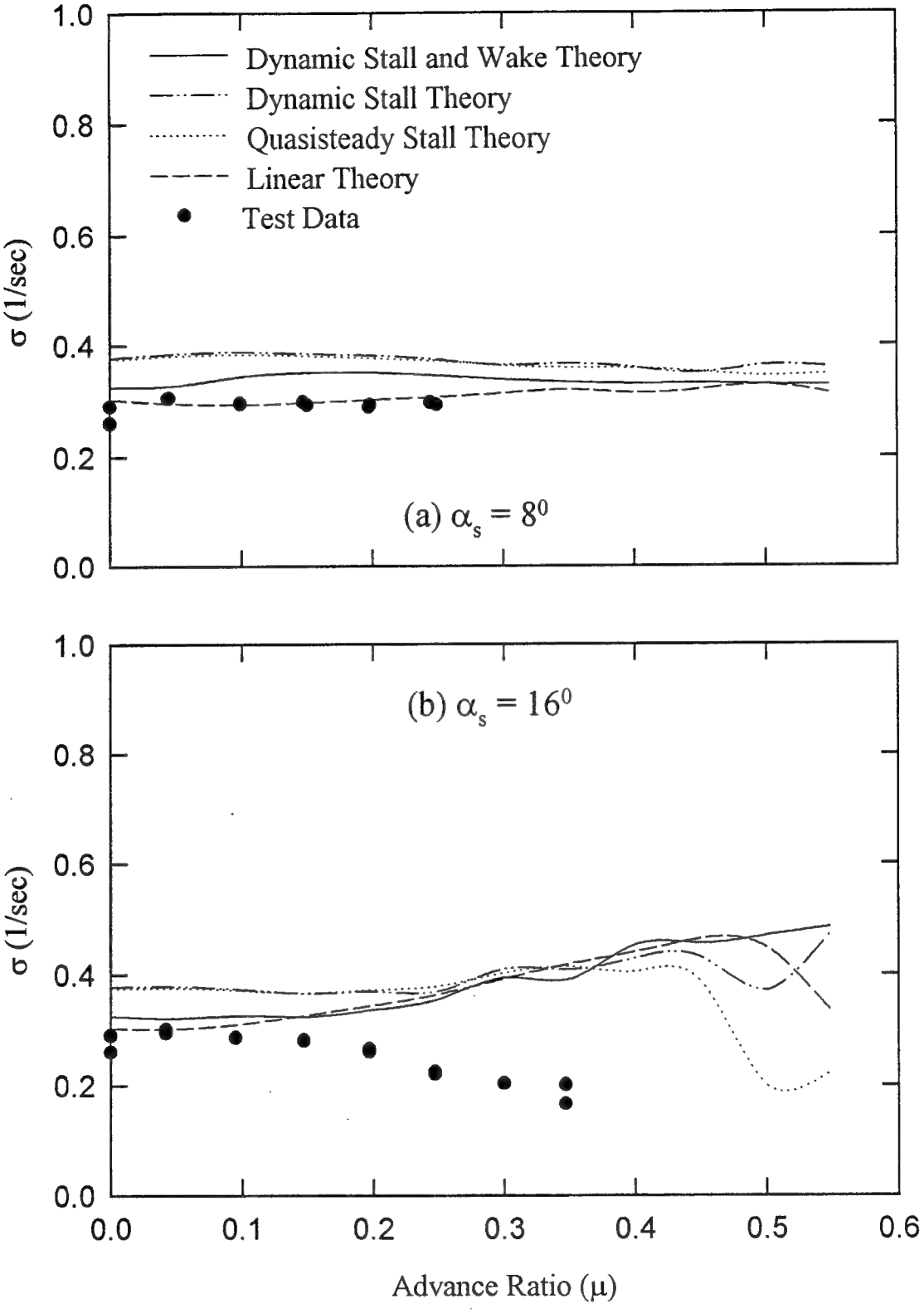

Figure 12: Effects of Aerodynamic Modeling on Lag-Damping Correlation from Modified Model for $\theta_0 = 3^0$.

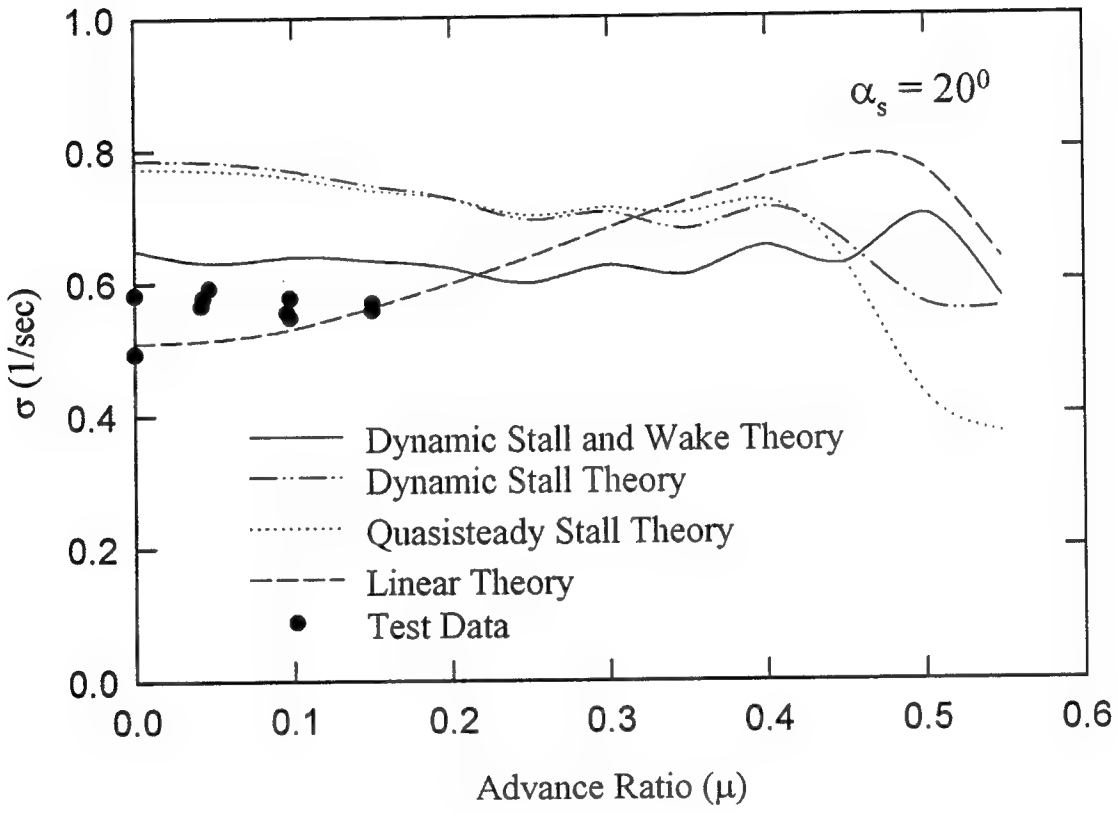

Figure 13: Effects of Aerodynamic Modeling on Lag-Damping Correlation from Modified Model for $\theta_0 = 6^0$.

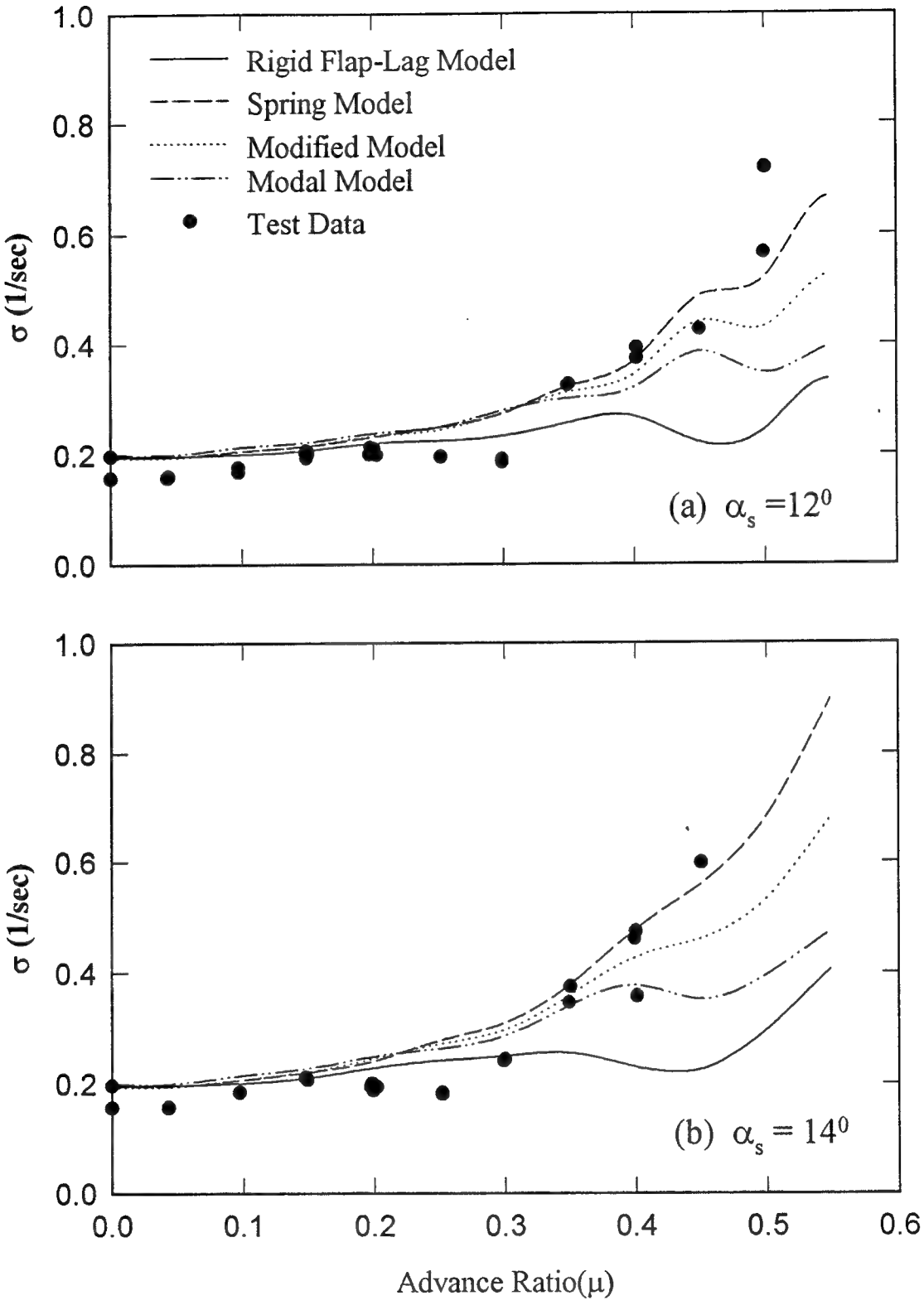

Figure 14: Effects of Structural Modeling on Lag-Damping Correlation from Dynamic Stall and Wake Theory for $\theta_0 = 0^0$ (concluded in the next page).

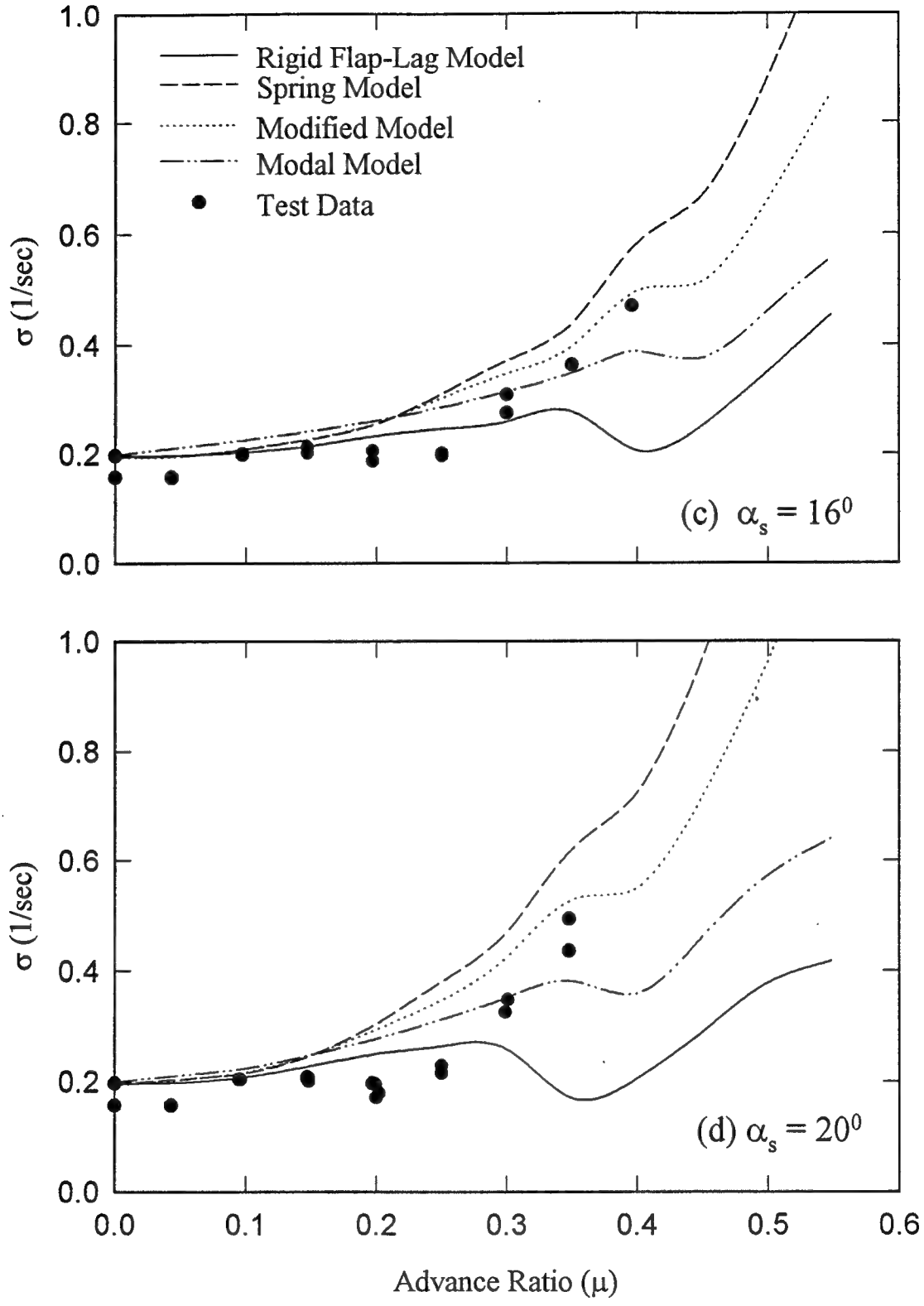

Figure 14 (continued): Effects of Structural Modeling on Lag-Damping Correlation from Dynamic Stall and Wake Theory for $\theta_0 = 0^0$.

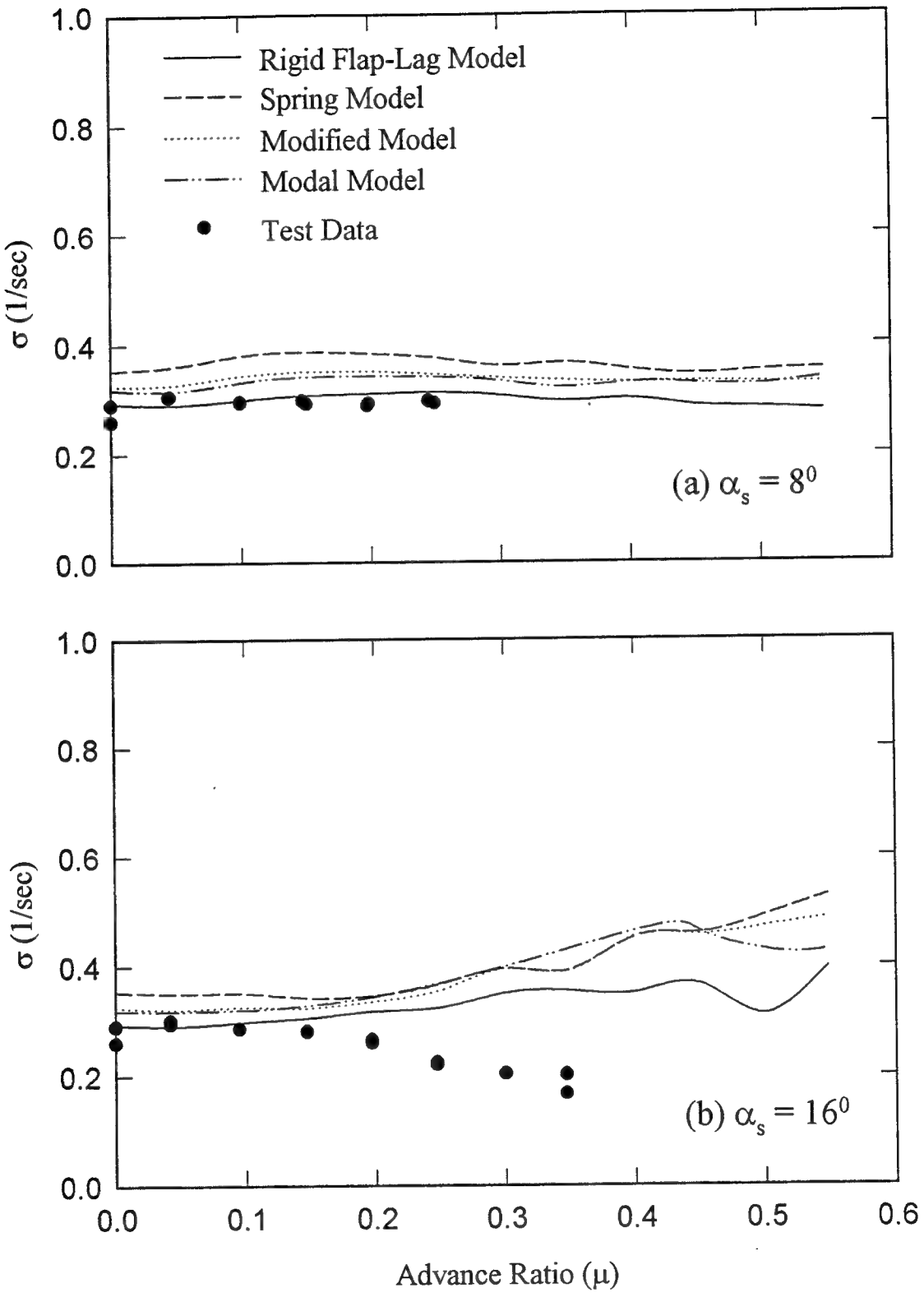

Figure 15: Effects of Structural Modeling on Lag-Damping Correlation from Dynamic Stall and Wake Theory for $\theta_0 = 3^0$.

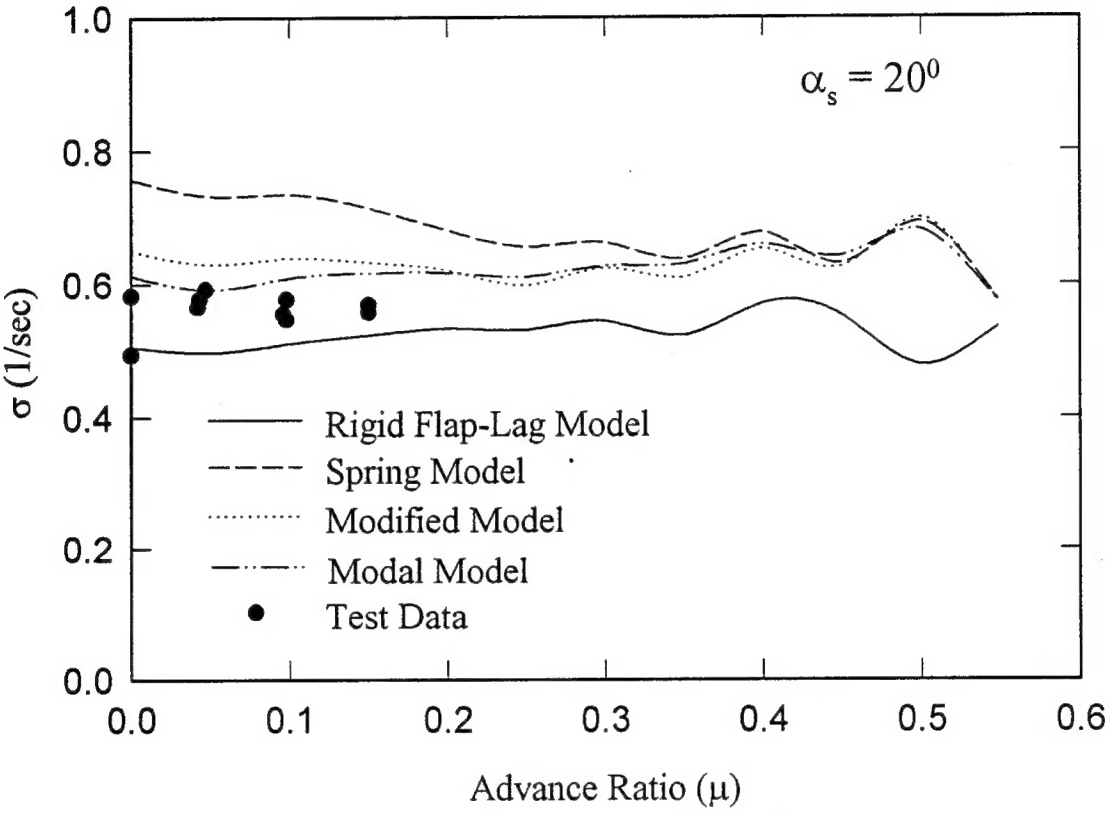

Figure 16: Effects of Structural Modeling on Lag-Damping Correlation from Dynamic Stall and Wake Theory for $\theta_0 = 6^0$.

List of Publications

Following is the list of manuscripts submitted or published under ARO sponsorship during the period of this research (including journal references).

1. Barwey, D. and Gaonkar, G. H., "Effects of Dynamic Stall and Structural Modeling on Helicopter Blade Stability with Experimental Correlation," Proceedings of the American Helicopter Society 48th Annual Forum, Washington, DC, Jun 3-5, 1992.

2. Achar, N. S. and Gaonkar, G. H., "Helicopter Trim Analysis by Shooting and Finite Element Methods with Optimally Damped Newton Iterations," *AIAA Journal*, Vol. 31, (2), Feb 1993.

3. Manjunath, A. R., Nagabhushanam, J., Gaonkar, G. H., Peters, D. A. and Su, A., "Flap-Lag Damping in Hover and Forward Flight With a Three-Dimensional Wake," *Journal of the American Helicopter Society*, Vol. 38, (4), Oct 1993.

4. Manjunath, A. R., Nagabhushanam, J., Gaonkar, G. H., Chunduru, Srinivas and Prasad Sampath, "Flap-Lag-Torsion Stability in Hover and Forward Flight With a Three-Dimensional Wake," Proceedings of the NASA-Ames/American Helicopter Society Aeromechanics Specialists Conference, San Francisco, CA, Jan 18-21, 1994.

5. Gaonkar, G. H., Nakadi, R. M., Subramanian, S. and Nagabhushanam J., "Parallel-Computing Concepts and Methods Toward Large-Scale Floquet Analysis of Helicopter Trim and Stability," Proceedings of the NASA-Ames/American Helicopter Society Aeromechanics Specialists Conference, San Francisco, CA, Jan 18-21, 1994.

6. Achar, N. S. and Gaonkar, G. H., "An Exploratory Study of a Subspace Iteration Method as an Alternative to the QR method for Floquet Eigenanalysis," *Mathematical and Computer Modeling*, Vol. 10, (3/4), 1994.

7. Barwey, D. and Gaonkar, G. H., "Dynamic-Stall and Structural-Modeling Effects on Helicopter Blade Stability with Experimental Correlation," *AIAA Journal*, Vol. 32, (4), Apr 1994.

8. Subramanian, S., Srinivas Chunduru, Gaonkar, G. H., "Effects of Dynamic Stall and Three-Dimensional Wake Effects on Aeroelastic Stability of Isolated Hingeless Rotors with Experimental Correlation," Proceedings of the American Helicopter Society 50th Annual Forum, Washington, DC, May 11-13, 1994.

9. Dang, Y. Y., Gaonkar, G. H., Prasad, J. V. R. and Hong Zhang, "Parallel Computing of Helicopter Response to Turbulence Toward Real-Time Implementation," Proceedings of the American Helicopter Society 50th Annual Forum, Washington, DC, May 11-13, 1994.

List of Personnel Supported

The estimated level of effort for this contract is about 65 man-months including the efforts of the principal investigator, Prof. Gopal H. Gaonkar. The personnel supported by this project are as follows:

1. Dr. Dinesh Barwey, Ph.D. degree completed in Spring 1992*.
2. Dr. N. S. Achar, Ph.D. degree completed in Spring 1992*.
3. Mr. R. M. Nakadi, M. S. degree completed in Fall 1994* (part of Fall 1993 and part of Spring 1994).
4. Mr. Y. Y. Dang, M.S. student, expected to graduate in December 1994* (Summer 92, part of Summer 1993 and Fall 1993).
5. Mr. S. Subramanian, Ph.D. student, since Spring 1991*.
6. Mr. S. J. Chunduru, Ph.D. student, since Spring 1991*.
7. Dr. J. Nagabhushanam, visiting scholar, May 1991-Jan 1992, Summer 1993.

*partially supported by the Mechanical Engineering Department, Florida Atlantic University.